International Journal of Solids and Structures 306 (2025) 113102

Contents lists available at ScienceDirect

International Journal of Solids and Structures

journal homepage: www.elsevier.com/locate/ijsolstr

Influence of block arrangement on mechanical performance in topological interlocking assemblies: A study of the versatile block

Tom Goertzen [a,*], Domen Macek [b], Lukas Schnelle [a], Meike Weiß [a], Stefanie Reese [b,c], Hagen Holthusen [b], Alice C. Niemeyer [a]

[a] RWTH Aachen University, Chair of Algebra and Representation Theory, Pontdriesch 10-16, 52062 Aachen, Germany
[b] RWTH Aachen University, Institute of Applied Mechanics, Mies-van-der-Rohe-Str. 1, 52074 Aachen, Germany
[c] University of Siegen, Adolf-Reichwein-Straße 2a, 57076 Siegen, Germany

ARTICLE INFO

Keywords:
Topological interlocking
Versatile block
FEM
Wallpaper symmetries
Directional blocking graphs
Interlocking flows
Mechanical investigation

ABSTRACT

Topological interlocking assemblies (TIA) are arrangements of blocks kinematically constrained by a fixed frame, such that all rigid body motions of each block are prevented by the neighbouring blocks and the frame. In the literature, several blocks are introduced that can be arranged into interlocking assemblies, however only few of them can be arranged in non-unique ways. This study investigates a particularly versatile interlocking block called the Versatile Block: this block can be arranged in three different doubly periodic ways given by wallpaper symmetries. We investigate the hypothesis that the arrangement of copies of the same block influences the mechanical response of a TIA. We examine the interlocking mechanism and the correlation between arrangement and overall structural performance in planar TIA consisting of the Versatile Block. Furthermore, we analyse load transfer mechanisms within the assemblies and from the assemblies onto the frame. For fast apriori evaluation of the load transfer onto the frame we introduce a combinatorial model called Interlocking Flows. To investigate our assemblies from a mechanical point of view we conduct several finite element studies. These reveal a strong influence of arrangement on the structural behaviour, for instance, an impact on both the point and amount of maximum deflection under a given load, thereby confirming our hypothesis. We also evaluate the accuracy of the proposed Interlocking Flow model by a comparison with the finite element simulations.

1. Introduction

The aim of resource efficiency and resource savings drives us to optimise not only the recyclability of everyday consumer goods but also the recyclability of components in the construction industry. Components are typically manufactured monolithically tailored to a specific application and consist of high performance composites. They require separation for recycling, which in most cases consumes additional energy. This raises the question of how to achieve resource efficiency without the need for recycling. One possible solution is to start at an earlier stage, namely to design buildings with reusable components. To achieve reusability, a transition from a monolithic approach to a modular design is required. Reusable components offer the potential of being assembled into different load-bearing structures. For example, components consisting of individual blocks that kinetically constrain each other and display structural load-bearing behaviour are particularly desirable.

The idea of building mortarless structures from blocks that kinematically constrain each other has been known for a long time. We are particularly interested in topological interlocking assemblies which give rise to planar mortarless structures.

A *topological interlocking assembly* can be defined as an arrangement of blocks that are in contact with each other together with a peripheral frame such that, if the frame is fixed, any non-empty finite subset of blocks of the assembly is prevented from moving, see Estrin et al. (2021). This kinematic restriction of movement is enforced by the neighbouring blocks. For a precise mathematical definition of topological interlocking assemblies, the reader is referred to Goertzen (2024b).

* Corresponding author.
E-mail addresses: tom.goertzen@rwth-aachen.de (T. Goertzen), domen.macek@ifam.rwth-aachen.de (D. Macek), lukas.schnelle1@rwth-aachen.de (L. Schnelle), weiss@art.rwth-aachen.de (M. Weiß), stefanie.reese@ifam.rwth-aachen.de (S. Reese), hagen.holthusen@ifam.rwth-aachen.de (H. Holthusen), alice.niemeyer@art.rwth-aachen.de (A.C. Niemeyer).

https://doi.org/10.1016/j.ijsolstr.2024.113102
Received 13 September 2024; Accepted 7 October 2024
Available online 20 October 2024

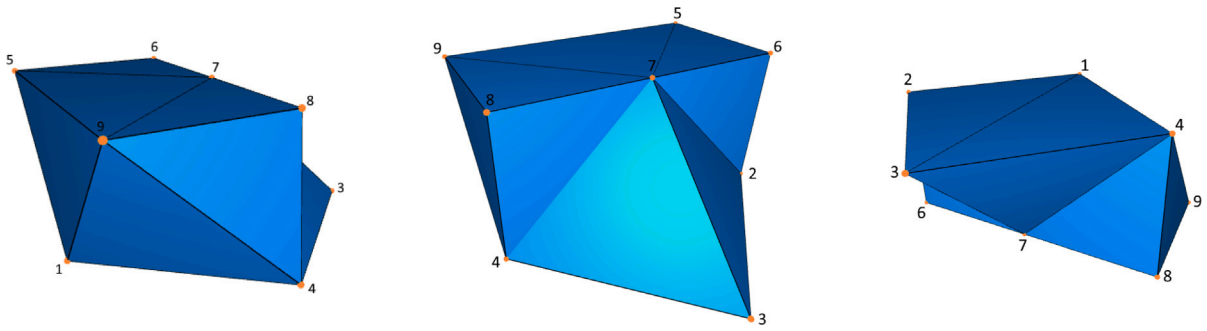

Fig. 1. Non-convex polyhedron, called *Versatile Block*, admitting topological interlocking assemblies with coordinates of vertices given by $v_1 = (0,0,0)$, $v_2 = (1,1,0)$, $v_3 = (2,0,0)$, $v_4 = (1,-1,0)$, $v_5 = (0,1,1)$, $v_6 = (1,1,1)$, $v_7 = (1,0,1)$, $v_8 = (1,-1,1)$, $v_9 = (0,-1,1)$.

1.1. State-of-the-art

The concept of topological interlocking assemblies (TIA), also known as topological interlocking materials (TIM) or topological interlocking structures (TIS), has a long history. It is related to the concept of masonry and the idea of building flat vaults. Early patents and concepts of blocks that admit a topological interlocking assembly can be found in the work of Abeille and Truchet in Gallon (1735) as well as Frézier (1738), who generalises the work of Abeille and Truchet. The block proposed by Abeille can be viewed as a truncated tetrahedron. Glickman (1984) proposes a paving block related to an assembly of tetrahedra. Dyskin et al. (2001a,b) initiate an investigation of topological interlocking assemblies as a novel material design concept and coin the term 'topological interlocking'. Moreover, they show that all Platonic solids give rise to topological interlocking assemblies (Dyskin et al., 2003a) and describe a method for constructing TIA with convex blocks (Kanel-Belov et al., 2010). Osteomorphic type blocks, which are introduced in Dyskin et al. (2003b), can also be assembled in various non-planar ways and this versatility gives rise to applications in civil engineering (see Dyskin et al., 2003b; Yong, 2011; Rezaee Javan et al., 2016; Harsono et al., 2023). Other methods for generating TIA linked to Voronoi tessellations are proposed in Subramanian et al. (2019), Akleman et al. (2020) and Mullins et al. (2022). Voronoi tessellations are naturally linked to crystallographic groups as certain (convex) Voronoi cells yield fundamental domains for such groups and thus space-filling structures, for example space-filling 'VoroNoodles' (Ebert et al., 2023).

A general method for constructing planar TIA based on non-convex fundamental domains of a crystallographic group is introduced in Goertzen et al. (2022) and Goertzen (2024a) and for non-planar TIA in Akpanya et al. (2023a). Recent overviews of design principles and applications related to TIA are given in Dyskin et al. (2019) and Estrin et al. (2021).

Several investigations in the literature focus on different aspects of the mechanical behaviour of TIA made of materials such as brittle materials (ceramics, concrete), metals (aluminium, steel) and plastics. An overview of the mechanical performance of TIA is given in Siegmund et al. (2016). Some also focus on developing new numerical models for studying TIA, e.g. Feldfogel et al. (2024a).

The studies by Krause et al. (2012) resp. Mirkhalaf et al. (2018) show that assemblies made of osteomorphic resp. convex ceramic blocks can withstand higher flexural deflection compared to monolithic solid ceramic plates—up to ten times — and outperform them in toughness—up to 50 times — while offering adjustable stiffness and resilience to damage. Mirkhalaf et al. (2018) also show that simultaneous improvements of strength and toughness is possible using a design based on octahedral blocks. Casting with concrete is a promising option for manufacturing blocks for TIA. Several mechanical experiments and simulations studying the behaviour of TIA with osteomorphic type concrete blocks are conducted in Rezaee Javan et al. (2017, 2018). Moreover, using soft-interfaces between blocks, for instance by applying rubber, Rezaee Javan et al. (2020) show that flexural compliance with less damage can be further improved.

Materials such as aluminium and steel are also promising materials when combined with the principle of TIA. Schaare et al. (2008) show that TIA, constructed from aluminium, steel or PVC cubes, demonstrate non-linear mechanical behaviours under indentation, including significant hysteresis, softening post-peak, and negative stiffness during unloading. This unique response is intrinsic to the assembly design, regardless of the material. Schaare et al. (2009) show that these interlocking assemblies also exhibit a unique, amplitude-dependent damping capacity due to friction between cube interfaces caused by mechanical vibrations.

Feng et al. (2015) investigate the impact mechanics of TIA with tetrahedra made of ABS and demonstrate numerically that these assemblies can absorb more impact energy than conventional solid plates.

TIA based on convex blocks can be parameterised using several methods, such as varying plane tessellations or angles of out-of planes. This yields a variety of TIA with distinct mechanical performance. For this, several parameter studies based on scaling convex blocks arising from various tessellations are conducted in Short and Siegmund (2019), Kim and Siegmund (2021), Williams and Siegmund (2021) and Weizmann et al. (2021).

Investigations of the effects of both the Young's modulus and the friction coefficient on the structural mechanics of TIA are investigated in Koureas et al. (2022) and Feldfogel et al. (2023, 2024b). Koureas et al. (2023) study the effect of non-planar block geometry in the context of beam-like structures. Ullmann et al. (2023) conduct a comparative study on the deflection limit of slab-like assemblies and monolithic slabs, and propose a theoretical upper bound on the deflection limit.

1.2. Hypothesis

Different blocks have been introduced that facilitate interlocking assemblies. Very few of these blocks can be arranged in different planar ways. This is a big restriction for modular systems. Goertzen et al. (2022) introduced a new block, called the *Versatile Block* (see Fig. 1), and Akpanya et al. (2023b) proved that this block can be arranged into interlocking assemblies in several different ways. *Whether the arrangement of copies of the same block also has an influence on the mechanical behaviour of an interlocking assembly was not yet known.* In this paper, we demonstrate that the mechanical behaviour of interlocking assemblies from the same block can differ greatly by comparing three different symmetric arrangements of the Versatile Block. For this, we introduce a new general combinatorial method, called 'Interlocking Flows', in the spirit of directional blocking graphs (Wang et al., 2018), that associates a flow network to an interlocking assembly and yields a fast prediction of the load transfer within the assembly. We compare the three different symmetric arrangements of the Versatile Block using the established method of FEM. Our focus lies on understanding the

dynamic interaction between the blocks within a planar assembly when subjected to transverse loading. We examine how external forces are transferred to the frame that holds the assembly together. To further improve our understanding of the topological interlocking assembly from a mechanical point of view, we conduct a comparative analysis of the load-bearing behaviour between the assemblies and monolithic plates of the same geometry, specifically evaluating the maximum deflection of the system and distribution of stresses under given load. The results of the FEM analyses confirm that the arrangement has an influence on the mechanical behaviour of the assembly and validate the novel method of Interlocking Flows.

2. Topological interlocking assemblies with the Versatile Block

Planar topological interlocking assemblies consist of blocks that are arranged between two parallel planes in 3D-space. We focus on planar interlocking assemblies consisting of identical blocks congruent to the *Versatile Block* (see Fig. 1), first introduced in Goertzen et al. (2022). For each assembly, the frame is chosen to consist of the blocks on the perimeter. The bottom-side of the Versatile Block forms a square in the plane $z = 0$ with area 2, whereas the top-side forms a rectangle in the plane $z = 1$ of the same area. In fact, the intersection of the Versatile Block with any plane $z = a$ with $a \in [0, 1]$ yields a polygon with area 2. We call the plane $z = 0$ the *bottom plane* and the plane $z = 1$ the *top plane*. Note that all vertices of the Versatile Block lie in either the top or the bottom plane.

Planar assemblies with the Versatile Block can be characterised by *Truchet tilings*, see Akpanya et al. (2023b). Here, a Truchet tile (see Smith and Boucher (1987)) is defined as a square with a diagonal such that one of the resulting triangles is coloured black and the other white and can be interpreted as a colouring of the bottom square of the Versatile Block, see Fig. 2. A Truchet tiling results in a corresponding assembly if any black triangle is adjacent only to white triangles and vice versa, see for instance Fig. 3. Using this correspondence it can be shown, that the Versatile Block can be arranged in 2^{n+m} possible ways in an $m \times n$ grid leading to exponentially many possible assemblies, see Akpanya et al. (2023b).

Out of these many possibilities, we select three symmetric arrangements, motivated by the fact that the construction of the Versatile Block corresponds to the wallpaper symmetries $p1$, pg and $p4$ (see Appendix B). We can assemble four copies of the Versatile Block according to these wallpaper symmetries, as shown in Fig. 3. These can be continued in a doubly periodic way to form infinite assemblies with the corresponding wallpaper symmetry, see Goertzen et al. (2022) and Goertzen (2024a). More on the underlying theory of arranging blocks with wallpaper symmetries is given in the Appendix B.

3. Interlocking flows

Recall that our aim is to compare the three different symmetric planar arrangements of the Versatile Block mentioned above to understand the interaction between the blocks and the frame within an assembly when subjected to transverse loading. FEM simulations are utilised in the following section to predict the mechanical behaviour of such assemblies precisely. Nonetheless, due to the time-intensive nature of FEM simulations, it is beneficial in engineering applications to forecast the quality of a topological interlocking assembly prior to a FEM simulation. In this section, the focus lies on the evaluation of the load transfer from the blocks onto the frame. For this, we introduce a fast discrete evaluation method based on the combinatorial theory of tilings and flow networks, which we call 'Interlocking Flows'.

The idea behind this tool is motivated by the principle of least resistance, or the principle that forces are taking the shortest path. Each block in the given assembly is associated to a node in a directed graph and for each arc (directed edge) in the graph we give a value. With this, each path in the graph can be quantified by multiplying the weights of each arc (see Example 3.3). Moreover, we show that the resulting system satisfies an equilibrium condition, i.e. applied loads are distributed within the network.

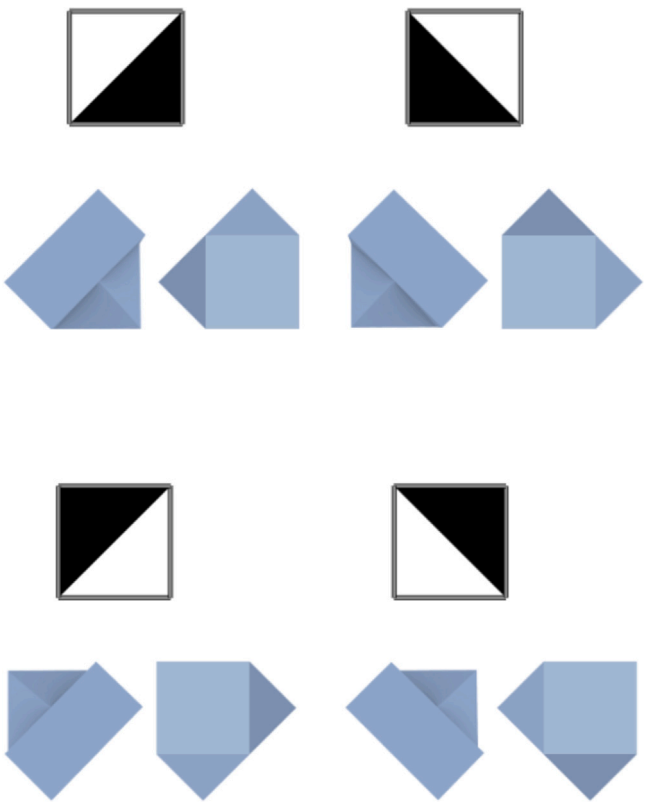

Fig. 2. Top: Orientations of a Truchet tile consisting of black and white triangle. Bottom: Top and bottom view of the corresponding orientation of Versatile Blocks, see Akpanya et al. (2023b). Possible arrangements of copies of the Versatile Block can be classified by the following tiling rule of Truchet tiles: adjacent tiles have to meet at different colours.

In more precise terms, we obtain a flow network that predicts the distribution of loads within the underlying assembly. For the underlying graph structure of this network, this method builds on the work on *Directional Blocking Graphs*, which are introduced in Wilson (1992) and Wilson and Latombe (1994) and investigated in the context of interlocking assemblies in Wang et al. (2018). Here, we give an adapted version of the definition of such a graph for interlocking assemblies by treating the blocks on the frame differently.

For this, let $(X_i)_{i\in I}$ be a topological interlocking assembly consisting of blocks $X_i \subset \mathbb{R}^3$ indexed by a finite index set I with a frame indexed by $J \subset I$ and $d \in \mathbb{R}^3$ a vector. We say that a block not contained in the frame is restrained in direction d by another block if shifting the first block in the direction d leads to an intersection with the latter block, i.e. for $i \in I \setminus J$ and $j \in I$, the translated block $X_i - d := \{x - d \mid x \in X_i\}$ intersects with X_j. Furthermore, we say that a block in the frame restrains itself from moving.

Definition 3.1. The *Directional Blocking Graph* (short *DBG*) $\mathcal{G}((X_i)_{i\in I}, d)$ is defined as the directed graph with

1. vertices given by the set I and
2. arcs of the form $i \to j$ if the block X_i is restrained by X_j in direction d for $i, j \in I$.

In the context of this paper, we apply a load x in the direction $d = (0, 0, -\varepsilon)$, for a small value $\varepsilon > 0$, for each block in the interlocking assembly simultaneously. We use the DBG to model how this load is

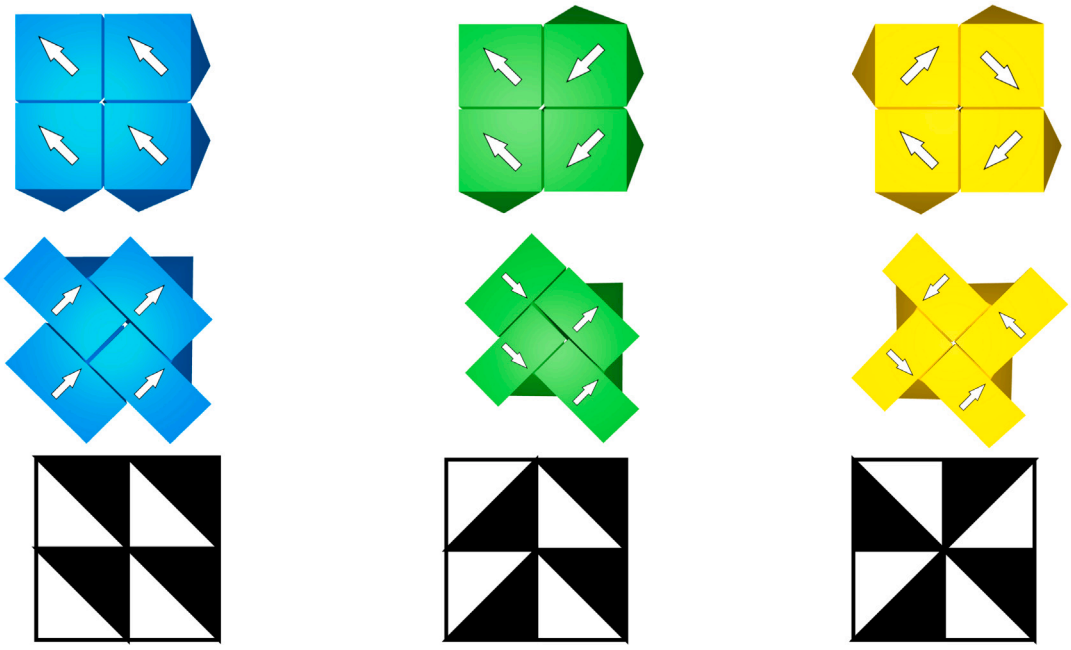

(a) $p1$ (b) pg (c) $p4$

Fig. 3. Bottom and top view with corresponding Truchet tiling of four copies of the Versatile Block arranged according to the wallpaper symmetries (a) $p1$, (b) pg and (c) $p4$.

transferred onto the frame of the underlying assembly. This can be achieved by introducing a value function on the arcs of a DBG, yielding a flow network with sinks given by the nodes corresponding to the blocks belonging to the frame.

Definition 3.2. Let $(X_i)_{i\in I}$ be a planar assembly with copies of the Versatile Block. We define a value function v for arcs of the DBG $\mathcal{G} := \mathcal{G}((X_i)_{i\in I}, d)$ with $d = (0, 0, -\epsilon)$ as follows: let $i \to j$ be an arc of $\mathcal{G}$ with $i, j \in I$, then we set

$$v(i \to j) := \begin{cases} \frac{1}{2}, & \text{if } i \neq j \\ 1, & \text{if } i = j. \end{cases}$$

Then $\mathcal{G}$ together with the value function v on its arcs is called an *Interlocking Flow*.

In the definition above, we choose the value $\frac{1}{2}$ for distinct Versatile Blocks, since in this context we assume that a given Versatile Block i in a given planar arrangement $(X_i)_{i\in I}$ is always supported equally by two of its neighbouring blocks from below. For blocks belonging to the frame, we choose the value 1, since these blocks are restrained from moving. Note that the definition of an Interlocking Flow can be easily generalised to assemblies with blocks other than the Versatile Block. Here, the value function v has to be chosen in a way such that the sum over all values of arcs leaving a given node is always equal to 1.

In the following, we restrict to the case, where I is given by a $n \times m$ grid for natural numbers n, m, where each square corresponds to an oriented Truchet tile which itself corresponds to an oriented copy of a Versatile Block and the frame consists of the outer blocks. It follows that the underlying assembly consists of $n \cdot m$ blocks.

We extend the value function v to any arcs $i \to j$ not contained in $\mathcal{G}$ by setting $v(i \to j) = 0$. With this choice of value function v it follows that $\sum_{j=1}^{n\cdot m} v(i \to j) = 1$, for all $i \in I$ and together with the fact that all values of v are non-negative, we obtain a (right) *stochastic matrix*

$$A = (v(i \to j))_{i,j\in I} \in \mathbb{R}_{\geq 0}^{n\cdot m \times n\cdot m}, \tag{1}$$

i.e. the entries of each row of A sum up to 1. This matrix can be viewed as a weighted *adjacency matrix* of the graph $\mathcal{G}$, yielding a flow network with capacity function v. This results in the following combinatorial interpretation: let $x \in \mathbb{R}_{\geq 0}^{I}$ be a load vector with $x_j = 0$, if $j \in J$ and $x_i \in \mathbb{R}_{\geq 0}$ for $i \in I \setminus J$. Thus, the entries of x correspond to the applied loads in direction d on each block. In the experiments depicted in the following, the entries of x are chosen to be $x_i = 1$ for $i \in I \setminus J$ and $x_j = 0$ for $j \in J$. The model of load transfer can then be discretised by considering the matrix–vector multiplication

$$A^k \cdot x$$

for iterations $k = 0, \dots, n$, where $\ell \gg 0$ is chosen to be large with $A^\ell \cdot x$ being close to the convergence load transfer on the frame given the initial load x. Since A is a stochastic matrix, it follows that the sum over all entries of $A^k \cdot x$ equals the sum over the entries of x, i.e.

$$\sum_{i=1}^{n\cdot m} (A^k \cdot x)_i = \sum_{i=1}^{n\cdot m} x_i,$$

which reflects the conservation property inherent to stochastic processes. We can exploit the underlying structure of the flow network to compute the matrix vector multiplication $A^k \cdot x$ as follows:

1. create an empty square grid corresponding to the Truchet tiling;
2. fill the box corresponding $i \in I$ with the value x_i (initialise vector x);
3. add $1/2$ times the value of box $i \in I \setminus J$ to box j if the white part of box i touches the black part of box j (this corresponds to the matrix multiplication $A \cdot x$);
4. iterate the second and third step $k - 1$ times with the updated boxes.

Example 3.3. In Fig. 4(a), we see an example of an Interlocking Flow Network corresponding to an assembly with 16 Versatile Blocks assembled according to the wallpaper symmetry pg, with 12 of them representing the frame, i.e. we have $n = m = 4$ with the notation as above. The Versatile Block corresponding to the grey nodes do not support any blocks from below, therefore there is no need to consider them. The remaining 8 Versatile Blocks are indexed by the set $\{I, \dots, VIII\}$ such that the blocks $\{V, VI, VII, VIII\}$ belong to the frame supporting the other blocks. The assembly of the blocks not belonging to the frame is also shown in Fig. 3(b). As discussed

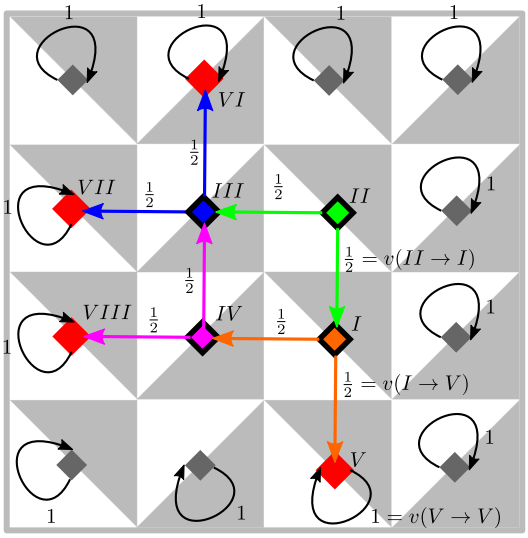

(a) Interlocking Flow for pg as given in Example 3.3. Nodes and arcs coloured in blue, green, orange and pink each represent one Versatile Block. Nodes coloured in red represent blocks belonging to the frame that support inner blocks from below. In the background, the corresponding Truchet tiling is displayed, illustrating the different orientations of the blocks. Note that the arcs in the DBG point from the white to the black regions in the Truchet tiling.

$$\begin{array}{c} \\ I \\ II \\ III \\ IV \\ V \\ VI \\ VII \\ VIII \end{array} \overbrace{\begin{array}{c} \begin{array}{cccccccc} I & II & III & IV & V & VI & VII & VIII \end{array} \\ \begin{pmatrix} 0 & 0 & 0 & \frac{1}{2} & \frac{1}{2} & 0 & 0 & 0 \\ \frac{1}{2} & 0 & \frac{1}{2} & 0 & 0 & 0 & 0 & 0 \\ 0 & 0 & 0 & 0 & 0 & \frac{1}{2} & \frac{1}{2} & 0 \\ 0 & 0 & \frac{1}{2} & 0 & 0 & 0 & 0 & \frac{1}{2} \\ 0 & 0 & 0 & 0 & 1 & 0 & 0 & 0 \\ 0 & 0 & 0 & 0 & 0 & 1 & 0 & 0 \\ 0 & 0 & 0 & 0 & 0 & 0 & 1 & 0 \\ 0 & 0 & 0 & 0 & 0 & 0 & 0 & 1 \end{pmatrix} \end{array}}^{=A}, \quad \overbrace{\begin{array}{c} \begin{array}{c} I \\ II \\ III \\ IV \\ V \\ VI \\ VII \\ VIII \end{array} \\ \begin{pmatrix} 1 \\ 1 \\ 1 \\ 1 \\ 0 \\ 0 \\ 0 \\ 0 \end{pmatrix} \end{array}}^{=x}$$

(b) Resulting matrix A, see Equation (1), and initial load vector x.

Fig. 4. Toy example for Interlocking Flows based on the assembly of Versatile Blocks based on wallpaper symmetries pg shown in Fig. 3(b).

above, each arc is given a positive value such that for each node, the values of all outgoing arcs sum up to 1. The values for the inner blocks are motivated by the fact that the blocks are symmetric, and we assume that they are supported by exactly two neighbouring blocks. For the outer blocks on the frame, we assume that they are restrained from moving and set the values to 1. The matrix shown in Fig. 4(b) results from the definition of the Interlocking Flow matrix A (1). For each of the inner blocks indexed by the set $\{I, II, III, IV\}$, we can apply a load in direction $d = (0, 0, -\varepsilon)$ for $0 < \varepsilon \ll 1$ small. The outer blocks belonging to the frame are not loaded. Assuming that all inner blocks are loaded by a value 1, we obtain a loading vector $x = (1, 1, 1, 1, 0, 0, 0, 0)$. Next, we can compute the distribution of x by computing the matrix–vector product $A \cdot x$. If we iterate this approach, we evaluate how x is distributed in an ith time step by computing the product $A^i \cdot x$, see Fig. 5. The final time step $A^4 \cdot x$ demonstrates the final distribution of load of the inner blocks transferred to the blocks belonging to the frame.

As mentioned in the previous section, the planar assemblies of copies of the Versatile Block are characterised by Truchet tiles. In Figs. 6–8, the Interlocking Flows for the wallpaper groups $p4$, $p1$ and pg are shown for assemblies with 10×10-blocks. For example, Fig. 6(a) displays an assembly with $p4$ wallpaper symmetry with $|I| = 100$ where the frame is marked in red. The corresponding Truchet tiling is given in Fig. 6(b). The initial starting distribution and more intermediate steps are shown using a heatmap displaying the load value distribution.

Remark 3.4. By considering the result obtained using the Interlocking Flow method, we can pick candidates for certain applications in a more time-efficient manner. For an 10×10 interlocking assembly with 100 for blocks, there are $2^{10+10} = 2^{20} = 1048576$ possible assemblies using the Versatile Block, see Akpanya et al. (2023b). For an initial prediction, we can evaluate the force transfer onto the frame for all 1048576 assemblies in a matter of seconds as it only revolves around matrix–vector multiplications with relatively small quadratic matrices, i.e. 100×100.

In Fig. 9 we show the corresponding Truchet tiling of an assembly with 50×50 Versatile Blocks. The computation of 1500 time steps take approximately 1.35 s on a personal computer with Apple M1 Chip. This example shows how this approach can be used for finding initial

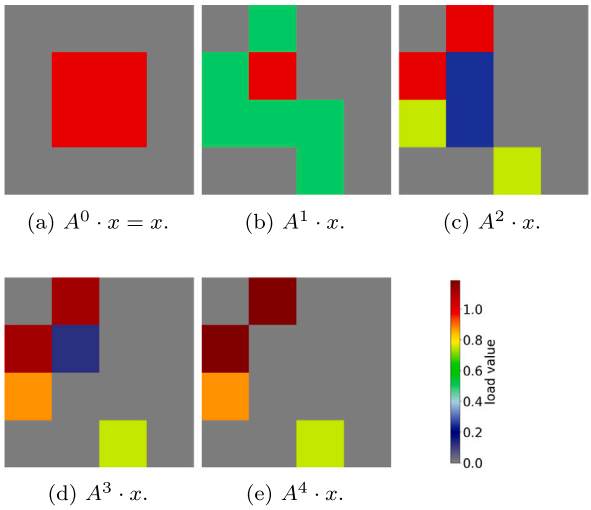

Fig. 5. Values for toy example in Fig. 4 that are obtained by computing the matrix–vector products $A^i \cdot x$, for $i = 0, \dots, 4$. The colours of the heatmaps indicate the corresponding values as given in the legend.

solutions for optimal designs and for efficiently predicting the load distribution from the assembly onto the frame.

4. Mechanical investigation of interlocking assemblies

4.1. Problem formulation

From the mechanical point of view, the blocks in the interlocking assemblies defined above are considered to be deformable bodies. External forces are applied to the blocks in the assembly causing them to move and deform. The blocks interact with each other only by the contact, which is unknown a priori and can change over time. In order to investigate purely the interlocking effect in the assemblies, we do not consider friction between the blocks. Neither the contact forces nor the displacements at the contact boundary of each block are prescribed. Thus, the geometry of the blocks must "constrain" the relative motion between them. This means that interlocking must be achieved only by the geometry of the blocks.

Mechanically, the problem can be formulated in the following way. The reference configuration $\Omega_0^{(k)} \subset \mathbb{R}^3$ of a body k denotes the domain occupied by all material points $\mathbf{X}^{(k)}$ at time $t = 0$. The changed positions $\mathbf{x}^{(k)}$ of a material point at a certain time t are described by the current configuration $\Omega_t^{(k)} \subset \mathbb{R}^3$. The displacement of a material point is described by $\mathbf{u}^{(k)}(\mathbf{X}^{(k)}, t) = \mathbf{x}^{(k)}(\mathbf{X}^{(k)}, t) - \mathbf{X}^{(k)}$. The boundary of each body $\partial\Omega_0^{(k)}$ is decomposed into three sets: $\Gamma_\sigma^{(k)}$ representing the Neumann boundary (tractions $\bar{\mathbf{t}}_0^{(k)}$ are given), $\Gamma_u^{(k)}$ representing the Dirichlet boundary (displacements $\bar{\mathbf{u}}^{(k)}$ are given), and $\Gamma_c^{(k)}$ representing the contact surface. Contact interaction can be mathematically interpreted as a set of nonlinear boundary conditions (see Laursen (2002) and Wriggers (2006)). The initial boundary value problem (strong formulation) of finite deformation elastodynamics needs to be satisfied on each body:

$$\operatorname{Div} \mathbf{P}^{(k)} + \tilde{\mathbf{b}}_0^{(k)} = \rho_0^{(k)} \ddot{\mathbf{u}}^{(k)} \qquad \text{in } \Omega_0^{(k)} \times [0, t], \tag{2}$$

$$\mathbf{u}^{(k)} = \bar{\mathbf{u}}^{(k)} \qquad \text{on } \Gamma_u^{(k)} \times [0, t], \tag{3}$$

$$\mathbf{P}^{(k)} \mathbf{N}^{(k)} = \bar{\mathbf{t}}_0^{(k)} \qquad \text{on } \Gamma_\sigma^{(k)} \times [0, t], \tag{4}$$

$$\mathbf{u}^{(k)}(\mathbf{X}^{(k)}, 0) = \bar{\mathbf{u}}^{(k)}(\mathbf{X}^{(k)}) \qquad \text{in } \Omega_0^{(k)}, \tag{5}$$

$$\dot{\mathbf{u}}^{(k)}(\mathbf{X}^{(k)}, 0) = \dot{\bar{\mathbf{u}}}^{(k)}(\mathbf{X}^{(k)}) \qquad \text{in } \Omega_0^{(k)}, \tag{6}$$

$$g_n^{(k)}(\mathbf{X}^{(k)}, t) \geq 0, \quad p_n^{(k)}(\mathbf{X}^{(k)}, t) \leq 0,$$

$$p_n^{(k)}(\mathbf{X}^{(k)}, t) g_n^{(k)}(\mathbf{X}^{(k)}, t) = 0 \qquad \text{on } \Gamma_c^{(k)} \times [0, t], \tag{7}$$

Table 1
Simulation parameters.

Parameter	Value	Description
ρ [kg m^{-3}]	7850	Density
E [GPa]	210	Young's modulus
ν [−]	0.3	Poisson's ratio
α [−]	2.0	Mass proportional damping
β [−]	$1.0 \cdot 10^{-8}$	Stiffness proportional damping

where $\mathbf{P}$ is the first Piola–Kirchhoff stress tensor, Div() denotes the Lagrangian divergence, and $\mathbf{N}$ is the normalised unit surface normal. The contact constraints in normal direction (7) for frictionless contact must hold on the contact boundary $\Gamma_c^{(k)}$ at each time t. Here, g_n is the gap function, and p_n is the contact pressure. The true internal stress state within a body is represented by Cauchy stress tensor $\boldsymbol{\sigma}$, which has the following relation to the first Piola–Kirchhoff stress tensor $\mathbf{P}$

$$\boldsymbol{\sigma} = \frac{1}{\det(\mathbf{F})} \mathbf{P}\mathbf{F}^T,$$

where $\mathbf{F}$ is the deformation gradient ($\mathbf{F} = \partial\mathbf{x}/\partial\mathbf{X}$).

Contact problems can be tackled using various numerical methods, such as finite element methods (FEM), discrete element methods (DEM), and multi-body systems. The selection of the appropriate method depends on the specific nature of the problem at hand. In our analysis, we choose the finite element method, as it is well-suited for examining the deformation and stress fields arising from quasi-static problems in assemblies composed of arbitrarily shaped solids. For a more in-depth explanation of FEM, we kindly refer interested readers to, e.g., Zienkiewicz et al. (2005) and Wriggers (2008) for general theory on FEM, and Wriggers (2006) and Laursen (2002) for computational contact mechanics.

4.2. Simulation setup

We analyse 3 different assemblies of 8×8 blocks that each correspond to the wallpaper-symmetries $p1$, pg and $p4$, respectively. The mechanical analyses were conducted by using the commercial finite-element software Abaqus/CAE 2022.HF1. As we are interested here in the static response of the three periodic arrangements of the Versatile Block, quasi-static analyses were carried out. The geometry of the Versatile Block is non-convex and complex, resulting in very complicated contact conditions between the blocks. Although we assumed that the deformations of the blocks are small (linear strain theory), they can still undergo finite rotations as there are 64 deformable bodies in the system. The complexity of such mechanical system is quite high, therefore an explicit dynamics environment was employed to increase the efficiency of the simulation and to account for the very general contact conditions.

To give the analysis a more realistic face, we scaled the coordinates of the Versatile Block and the resulting assemblies (Figs. 6(a), 7(a), 8(a)) by a factor of 0.2, where we interpret the length units as metres and thus obtain a block of height 0.2 m. In this case, the side-length of the square equals $0.2 \cdot \sqrt{2} \approx 0.283$ m. Especially, a 10×10 assembly (including the frame) of scaled Versatile Blocks in a square grid will be of size $\approx 2.83 \times 2.83$ m^2.

In order to understand the key mechanical advantages and disadvantages of the underlying TIA, we compare their mechanical properties with corresponding monolithic plates of the same dimensions.

We considered the bodies as isotropic and linear elastic material, which properties are listed in Table 1. The soft, frictionless contact between all the bodies was defined using an exponential pressure-overclosure relationship. According to the Abaqus definitions, the following parameters were set: a clearance between the bodies, $c_0 = 10^{-7}$ m (measured in the contact normal direction), and a contact pressure at zero clearance, $p_{c_0} = 10^3$ Pa. All blocks were meshed individually with 4-node tetrahedral elements (see Fig. 11). The displacement boundary

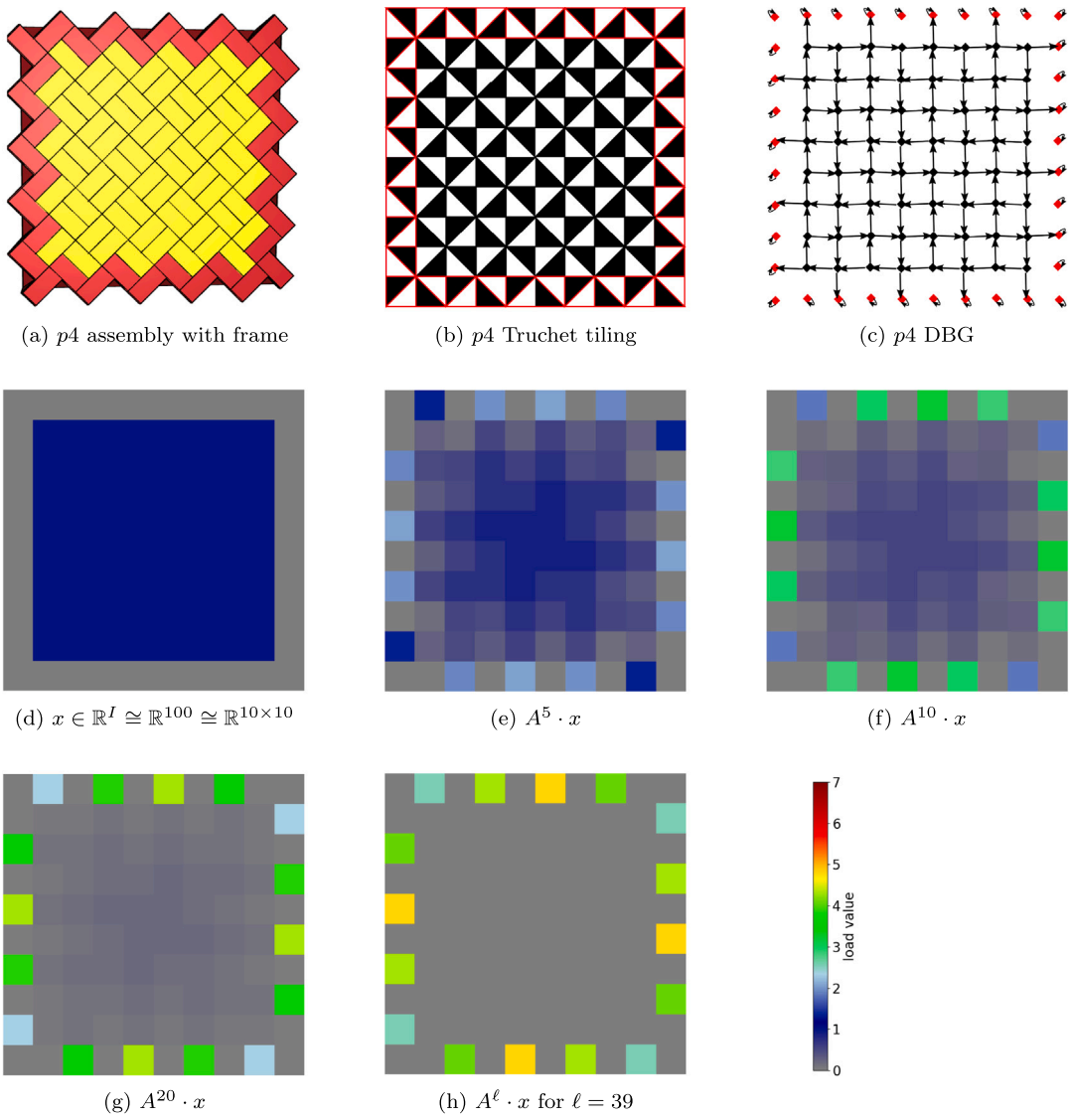

(a) $p4$ assembly with frame (b) $p4$ Truchet tiling (c) $p4$ DBG

(d) $x \in \mathbb{R}^I \cong \mathbb{R}^{100} \cong \mathbb{R}^{10\times 10}$ (e) $A^5 \cdot x$ (f) $A^{10} \cdot x$

(g) $A^{20} \cdot x$ (h) $A^\ell \cdot x$ for $\ell = 39$

Fig. 6. In (a), we see the arrangement of Versatile Blocks according to $p4$ wallpaper symmetries, with the frame marked in red. In (b), the corresponding Truchet tiling is shown. The Interlocking Flow analysis is based on the Directional Blocking Graph (DBG) in (c), with arc values as given in Definition 3.2. The results of the Interlocking Flow are displayed for different discrete time steps in (d)–(h).

conditions were applied by fully fixing (in all their nodes) the peripheral blocks (the bounding frame) in space (see Fig. 10). A pressure of $p_0 = 1.5\,\text{bar}$ transversely to the assembly plane was applied onto the top plane (see Fig. 10) using the integrated function "smooth step", which automatically produces smooth load amplitude. This function prevents sudden movements, which can cause stress waves that can lead to noisy or inaccurate solutions. Quasi-static loading conditions were considered. Both a damping term related to the volumetric strain rate and the square of the volumetric strain rate were considered. Material damping has been used to dampen lower (mass-dependent) and higher (stiffness-dependent) frequency responses (see Table 1). To perform the quasi-static analysis more efficiently, mass scaling was also employed to increase the integration time step. This resulted in a corresponding reduction of computational time. In order to ensure that changes in mass and resulting increases in inertial forces would not significantly alter the solution, the mass scaling factor was chosen appropriately by testing (mass scaling factor of approx. 10). All Abaqus input files can be found in Goertzen et al. (2023) (https://doi.org/10.5281/zenodo.10246034).

4.3. Numerical results

Contact pressure. One of the most important questions regarding the interlocking mechanism is: *How is an external load transferred through the assembly to the bounding frame?* This question has already been addressed, for example, in the works of Khandelwal et al. (2012, 2013), Rezaee Javan et al. (2020), Akleman et al. (2020). We also dealt with this question in the last section, where Interlocking Flows were used to analyse interlocking mechanism. Here, we examine this question from a mechanical point of view. To do this, we investigate the contact pressure between the blocks and the frame, since we assumed that there is no friction involved. The contact pressure ($p_0 = F/A$) indirectly represents the distribution of forces in a TIA (between the blocks).

The results are shown in Fig. 12. Unlike the monolithic plate, the assembly transfers the load by pressure. In the top plane ($z = 0.2\,\text{m}$) of $p1$, the highest contact pressure occurs in the central part of the diagonal of the TIA. In this plane, the contact pressure between the assembly and the right and top edges of the frame is also the highest. In the bottom plane ($z = 0.0\,\text{m}$) the highest pressure occurs only at the left and lower edges of the frame. The simulations show that load transfer of $p1$ occurs over the two boundary edges in the bottom plane

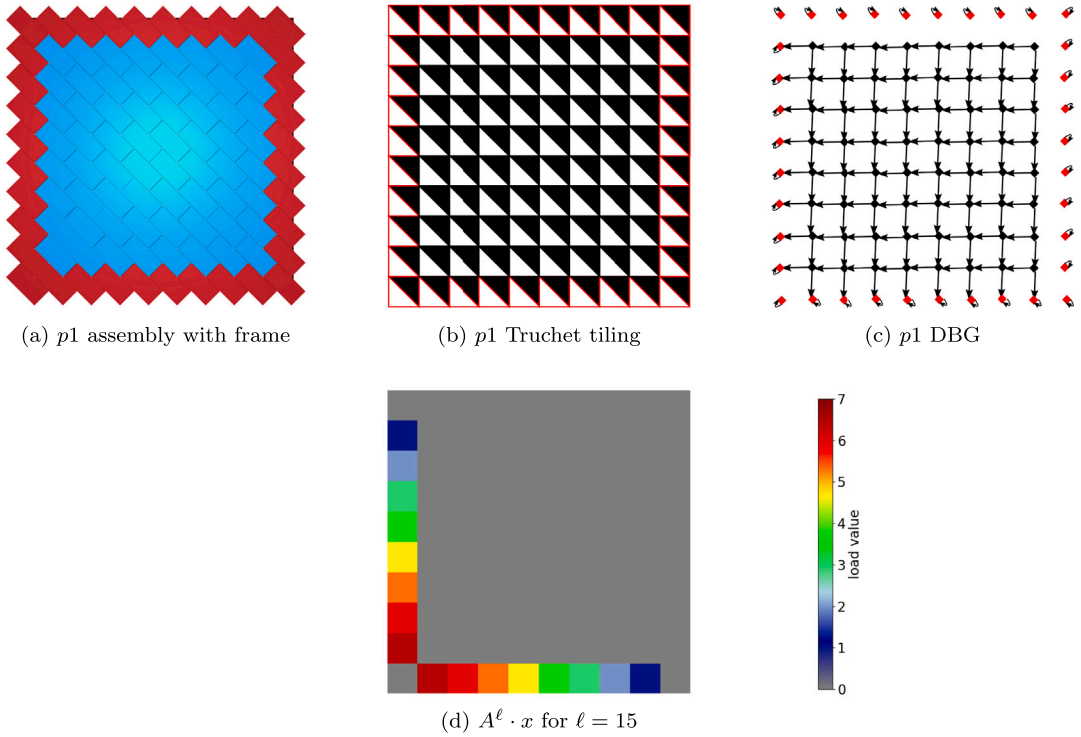

(a) $p1$ assembly with frame (b) $p1$ Truchet tiling (c) $p1$ DBG

(d) $A^{\ell} \cdot x$ for $\ell = 15$

Fig. 7. In (a), we see the arrangement of Versatile Blocks according to $p1$ wallpaper symmetries, with the frame marked in red. In (b), the corresponding Truchet tiling is shown. The Interlocking Flow analysis is based on the Directional Blocking Graph (DBG) in (c), with arc values as given in Definition 3.2. The results of the Interlocking Flow are displayed for the convergence time step given in (d).

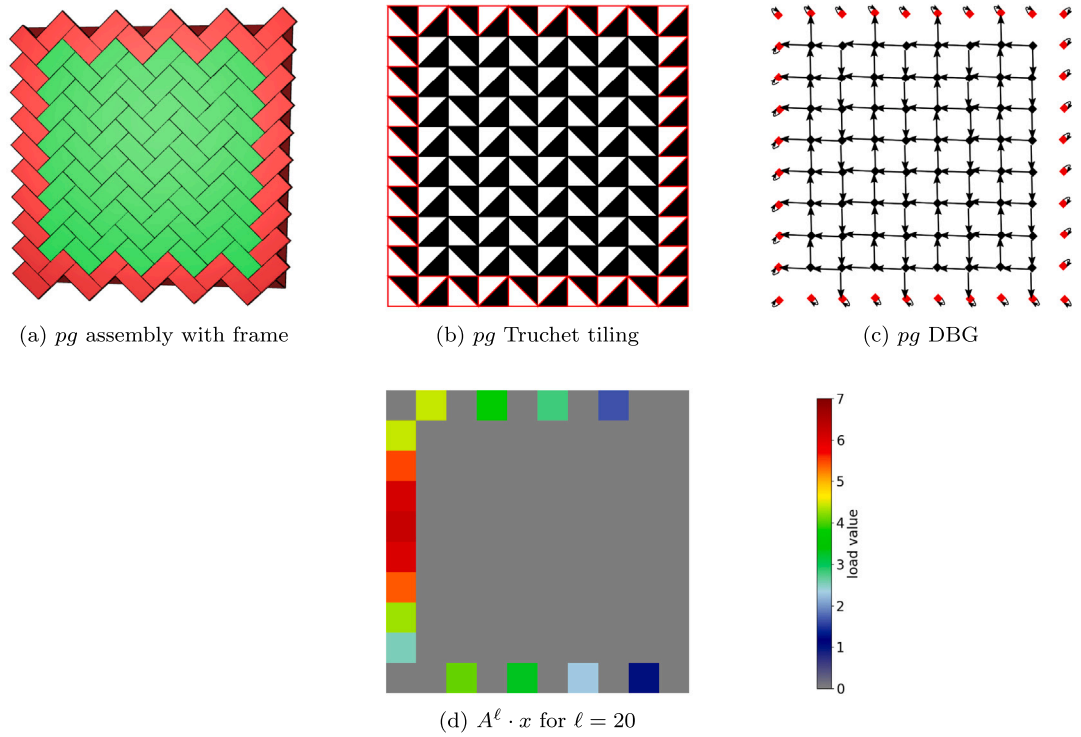

(a) pg assembly with frame (b) pg Truchet tiling (c) pg DBG

(d) $A^{\ell} \cdot x$ for $\ell = 20$

Fig. 8. In (a), we see the arrangement of Versatile Blocks according to pg wallpaper symmetries, with the frame marked in red. In (b), the corresponding Truchet tiling is shown. The Interlocking Flow analysis is based on the Directional Blocking Graph (DBG) in (c), with arc values as given in Definition 3.2. The results of the Interlocking Flow are displayed for the convergence time step given in (d).

and the two opposing boundary edges in the top plane (see first column in Fig. 12).

In the top plane ($z = 0.2$ m) of pg, the highest contact pressure occurs in the centre right part of the TIA. In this plane, the pressure between

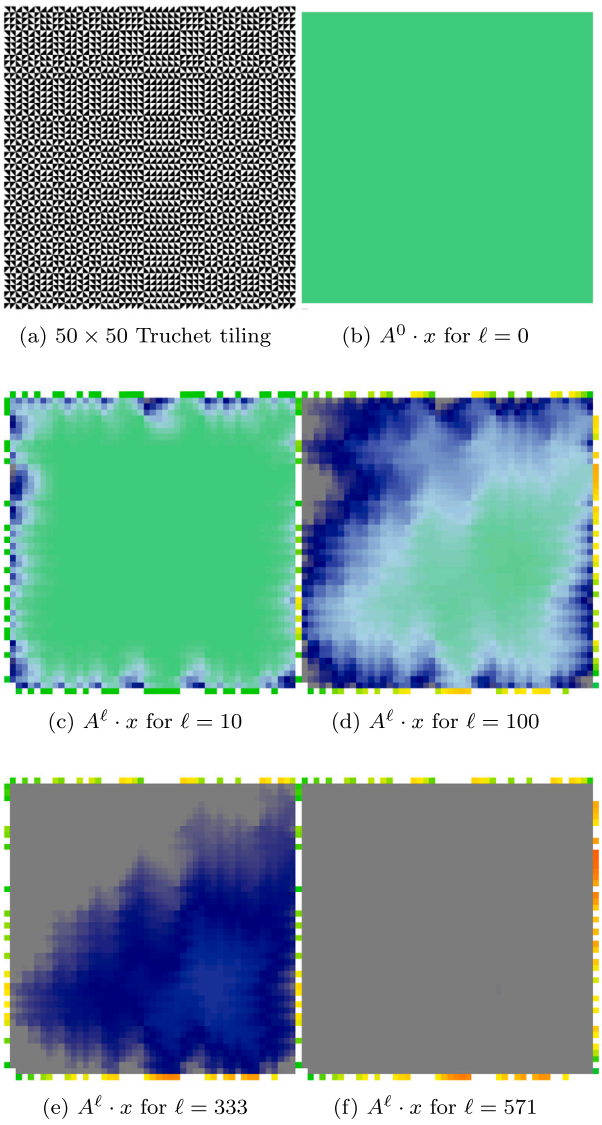

Fig. 9. This figure illustrates the Interlocking Flow method applied to a large assembly of 50 × 50 Versatile Blocks, corresponding to the tiling with Truchet tiles shown in (a). Different time steps (b)–(f) show the evolution of load distribution over discrete iterations. In the final time step (f), we see the modelled load distribution onto the frame.

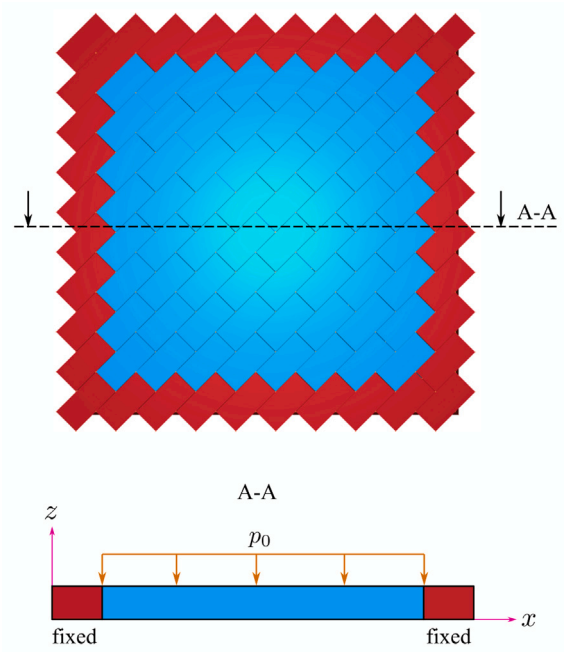

Fig. 10. Schematic illustration of boundary conditions applied to the TIA of interest. Peripheral blocks (red), which form the frame, are fixed in space. The *p*1 arrangement of Versatile Blocks (blue) is constrained by the frame. A pressure p_0 is applied to the top plane of the assembly (blue region). Boundary conditions are applied to the *pg* (Fig. 8(a)) and *p*4 (Fig. 6(a)) assemblies in a similar way.

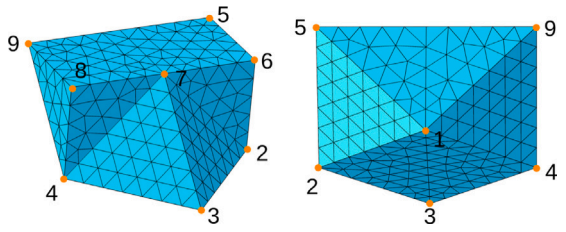

Fig. 11. Finite element discretisation (mesh) of one Versatile Block.

the assembly and the right edges of the frame is also the highest. In the bottom plane ($z = 0.0$ m), the highest pressure occurs at the left, lower and upper edges of the frame. Here, too, the assembly is supported by the frame in both the top and bottom planes. We also observe that in bottom plane, only every second block is highly stressed at the lower and upper edges of the frame. This means that not all blocks with direct contact to the frame transfer the forces to the frame (see second column in Fig. 12).

In the top plane ($z = 0.2$ m) of *p*4, the highest contact pressure occurs in the centre part of the TIA forming an "X". In this plane, the pressure between the assembly and the edges of the frame is low. In the bottom plane ($z = 0.0$ m), the highest contact pressure occurs at all four edges of the frame. In contrast to the other two assemblies, the assembly is only supported by the frame in the bottom plane. Similar to the *pg* assembly, we notice that in the bottom plane only every second block is highly stressed at the edges of the frame, which means that not all blocks at the frame transfer the forces to the frame (see third column in Fig. 12).

Due to the symmetry of the Versatile Block and the assemblies, symmetry can also be observed in the contact pressure distribution. In the *p*4 assembly, the four-fold symmetry of the underlying wallpaper symmetry is still present as highlighted by the black-square. Moreover, in the *p*1 assembly we see a reflection symmetry along the diagonal highlighted by the black-line. The case *pg* is more involved as the assembly is arranged using glide reflections this leads to a shift of the high stresses at the frame (note that a glide reflection is composed of a reflection together with a translation/shift).

If we compare the FEM results (second row in Fig. 12) with the results of the interlocking flow method (see Fig. 7, Fig. 8, Fig. 6), we observe that the interlocking flow method accurately predicts which blocks in the assembly are responsible for transferring the load to the bounding frame, see Fig. 13. The locations of contact pressure peaks in the FEM simulation align with those identified by the interlocking flow method. However, the density of the force transferred from the block does not match the FEM simulation results, particularly in the p1 TIA. This discrepancy can be attributed to the slipping behaviour of the blocks (Khandelwal et al., 2013; Djumas et al., 2017; Koureas et al.,

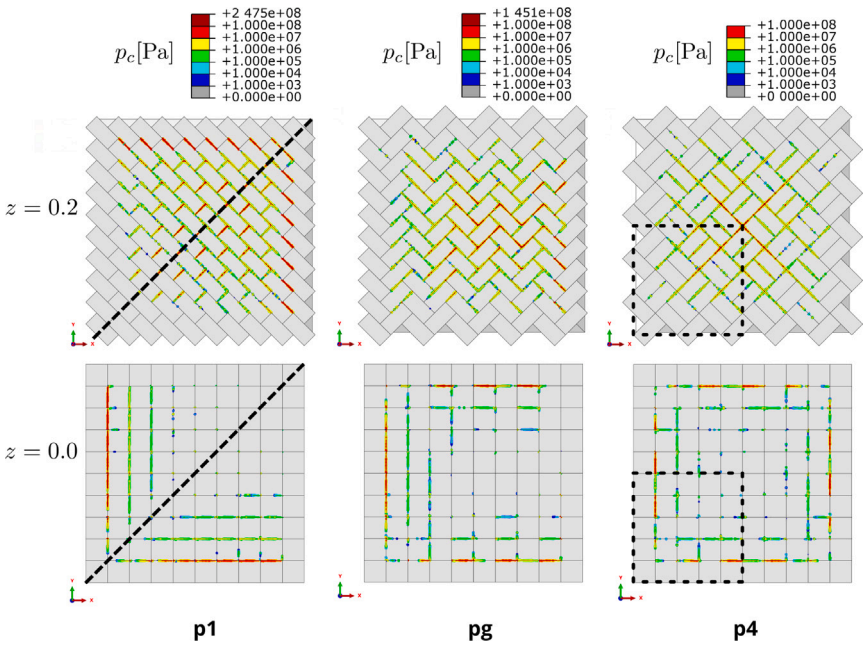

Fig. 12. Contact pressure (FEM simulation) between the blocks in the TIA of interest. The first row represents the top plane, and the second row represents the bottom plane. Due to the symmetry of the Versatile Block and the assemblies, symmetry can also be observed in the contact pressure distribution. In the $p4$ assembly, the four-fold rotational symmetry around the centre of the assembly of the underlying wallpaper symmetry is highlighted by the black square. Additionally, in the $p1$ assembly, a reflection symmetry along the diagonal is highlighted by the black line.

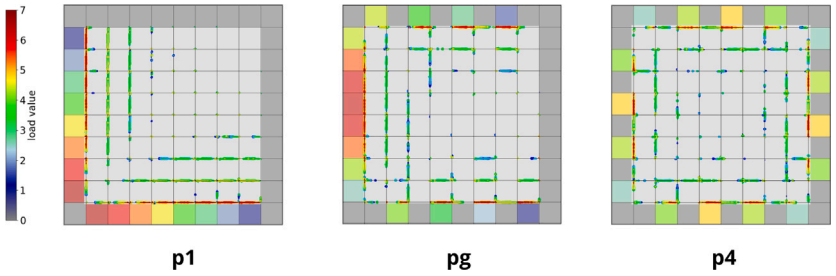

Fig. 13. A direct comparison between the Interlocking Flow results and the contact pressure results from the FE simulation is shown. The Interlocking Flow results are overlaid on the FE simulation contact pressure data, allowing a direct visual comparison between the two sets of results. Note that the locations of contact pressure peaks correspond with the force magnitudes imposed on the frame as obtained using the interlocking flow method.

2022), including rotation and deformation, which the interlocking flow method neglects.

From each TIA, we extracted information from a single block near the centre of the assembly to gain insight into how the blocks interact and interlock with each other. To illustrate this, we plotted the contact pressure on the surface of the block. These results are shown in Fig. 14. The block around the centre of the assembly was chosen for this analysis because high contact pressure consistently occurs around the centre of the top plane for all TIA.

From these results, it is clear to see how blocks interact with each other differently in different arrangements. The results namely show which regions of the block transfer the forces in the assembly. They also show which regions might lead to weaknesses and failures within the block. The interactions are directly connected to the wallpaper symmetries (see 3(a), 3(b) and 3(c)). For instance, in the $p1$-assembly the interaction can be represented with only one block. The region "1" in front (Fig. 14) interacts with the region "1" in the back of the block, edge "2" in the front with the edge "2" in the back, or region "3" in the front with region "3" in the back and so on. Similarly, the interaction in $p4$ can also be easily described, but for pg the description becomes much more complex.

For all three arrangements, the highest contact pressure occurs mainly in the upper part of the block. The lower parts of the blocks are less loaded. This has a direct influence on the von Mises stress distributions, which can be seen in Fig. 16.

The primary aim of this study is to gain initial insights from the simulation. From these results, we can gather some understanding of the behaviour of the arrangements. However, a more detailed investigation is certainly necessary to fully understand the interactions between the blocks, as well as between the frame and the assembly. Such an analysis, however, is beyond the scope of this work.

Deformed state and maximum deflection at a given load. Fig. 15(a) shows the displacement fields u_z in z-direction of the three TIA. The displacement u_z is shown because the deformation in z-direction is most dominant due to the loading direction. The deformation patterns of the interlocking assemblies follow the patterns and the directions of the monolithic plates (Fig. 15(b)) but behave slightly differently due to the modular nature of the assemblies. In $p1$, the displacement field spreads along the diagonal from the bottom left corner to the top right corner. The reason for this deformation is that all blocks have the same orientation. In pg, the deformation spreads from the left boundary in the positive x-direction and is limited by the top and bottom boundaries. In $p4$, the deformation is equally distributed in all directions and therefore the maximum deflection occurs in the middle. The displacements of the blocks in $p1$ at the left and bottom boundary (in purple in Fig. 15(a))

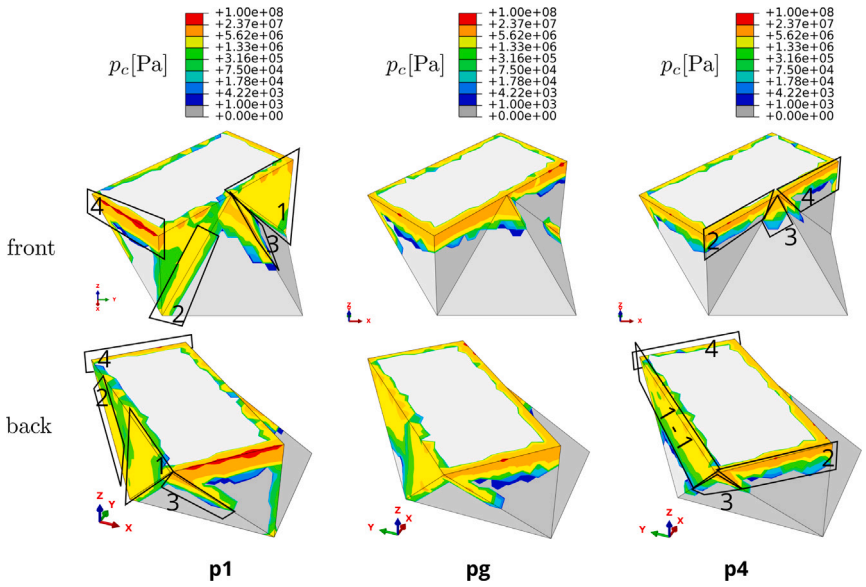

Fig. 14. Contact pressure on the block around the centre of each TIA. The first row shows the front side of the Versatile Block, while the second row shows the back side. The first column plots the contact pressure distributions on the block in the $p1$ assembly, the second column plots the pressure distributions in the pg assembly, and the third column plots the distributions in the $p4$ assembly. The numbered regions on the blocks in the $p1$ and $p4$ assembly indicate which areas of the block interact with corresponding areas on another block.

are positive, which suggests that their neighbouring blocks leverage them out. This behaviour differs from that of the solid plate. Similar differences between the solid plate and the assemblies pg and $p4$ can be observed. The comparison of the maximum deflections of TIA with the solid plates shows that the $p1$ arrangement performs surprisingly better, while pg and $p4$ arrangements perform about 50% worse. The maximum deflection occurs in front of the right corner block in $p1$; slightly to the right of the centre for pg; and in the centre for $p4$. The results show that there is a difference in the displacement distribution between the top and bottom plane of the TIA. Overall, it can be concluded that the choice of arrangement and frame control the position of the maximum deflection at a given loading.

Distribution of stresses. Fig. 16 shows the distribution of von Mises stresses in the assemblies. The stress distribution is very complex, which can be associated with the non-convex geometry of the block. For comparison, the stress distributions in corresponding solid plates are shown in Fig. 17, which are shaped according to the frames of the different assemblies. Particularly interesting is the distribution of stresses from the top plane, where the load is applied, to the bottom plane. The results show that different block arrangements strongly influence the stress distribution in the assembly.

The results show (Fig. 16) that in all three assemblies the highest von Mises stresses occur at the contacts between the blocks. Therefore, we do not compare the maximum von Mises stresses occurring in the TIA, as these result from small contact areas that evolve during the deformation of the entire assembly. Nevertheless, we can make observations about how contact pressure influences the stress distribution through the assembly.

Due to the symmetry of the Versatile Block and the assemblies, symmetry can also be observed in the stress distribution. For instance, in the $p4$ assembly, the four-fold rotational symmetry of the underlying wallpaper symmetry is still present in the stress distribution as highlighted by the black-square (Fig. 16). Moreover, in the $p1$ assembly we see a reflection symmetry along the diagonal highlighted by the black-line.

In the top plane of $p1$, contacts form the highest stresses in the central part of the diagonal of the TIA and between the assembly and the right and top edges of the frame. In the bottom plane, the highest stresses occur only at the left and lower edges of the frame. The stresses on the diagonal (from the bottom edge to the right edge) gradually decrease as one moves from the top to the bottom plane. It can also be seen that the lower left block (in the corner) is hardly stressed.

In the top and bottom plane of pg, the highest stresses also occur where the highest contact pressure is: in the centre right part of the TIA and between the assembly and the right edges of the frame and at the left, lower and upper edges of the frame. At the right edge of the frame in the bottom plane, the middle blocks are more stressed than the upper and lower ones. The stresses in the middle and right part of the assembly gradually decrease as one moves from the top to the bottom plane.

In the top and bottom plane of $p4$, the highest stresses occur in the centre part of the TIA. They form an "X". In this plane, the stresses between the assembly and the edges of the frame are low. In the bottom plane, the highest stresses occur at all four edges of the frame. The stresses in the centre of the assembly gradually decrease as one moves from the top to the bottom plane.

Similar observations can also be made for the reference solutions (Fig. 17). For all three monolithic plates, the highest von Mises stresses occur at the contact points between the plate and the frame. This is a consequence of the sharp, non-straight edges of the plate and the assembly.

In comparison to the monolithic plates the stress distributions in TIA are discontinuous, which is not surprising at all, since the assemblies are composed of independent bodies. Due to the contacts between blocks, the top plane experiences more stress than the bottom plane. In $p1$, the von Mises stresses reach up to 30 MPa (indicated by the yellow and orange regions in the plots). These high-stress regions are much larger than those in pg and $p4$. In comparison, the monolithic $p1$-plate reaches stresses up to 18 MPa, while in pg-plate the stresses reach 11 MPa, and in $p4$-plate they reach 7 MPa. Major differences can be observed below the middle plane $z = 0.1$ m. As expected, the most blocks in the assemblies are less stressed compared to the same regions in the monolithic plates. This is because the gap between neighbouring blocks opens, causing a loss of contact. In the $p1$ assembly, stresses range between 0 and 18 MPa (excluding the blocks in contact with the frame). In the pg and $p4$ assemblies, stresses range between 0 and 4 MPa. In the $p1$ plate, stresses range between 4 and 19 MPa, while in the pg plate, they range between 1 and 11 MPa, and in the $p4$ plate, they range between 1 and 7 MPa. Another significant difference can be observed

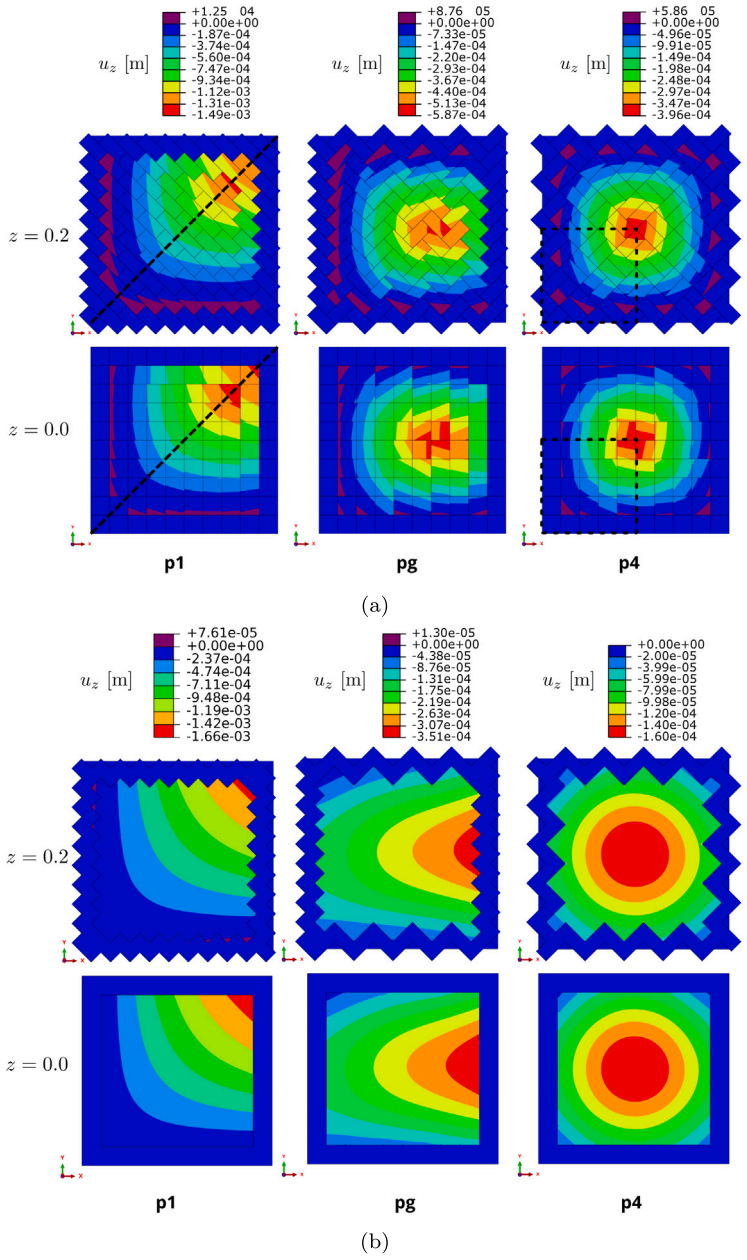

Fig. 15. This figure shows displacement fields in z-direction in the top ($z = 0.2$ m) and bottom ($z = 0.0$ m) plane of the three TIA (a) and three monolithic plates (b). In the $p1$-arrangement, the maximum displacement occurs at the top right. The shape of the displacement contours appears to be "hyperbolic". The maximum displacement in pg-arrangements occurs in the middle right part of the assembly. The contours of the displacements have a "parabolic" shape. The maximum deflection in $p4$-arrangements is formed in the centre of the assembly and the contours of the displacements have a "circular" shape. The lowest maximum deflection of 0.396 mm is in $p4$, the highest in $p1$ at 1.49 mm. Due to the symmetry of the Versatile Block and the assemblies, symmetry can also be observed in the displacement fields. In the $p4$ assembly, the four-fold rotational symmetry around the centre of the assembly of the underlying wallpaper symmetry is highlighted by the black square. Additionally, in the $p1$ assembly, a reflection symmetry along the diagonal is highlighted by the black line. In the $p1$-like plate, the maximum displacement occurs at the top right. The shape of the displacement contours appears to be "hyperbolic". The maximum displacement in pg-like plate occurs in the middle right part of the assembly. The contours of the displacements have a "parabolic" shape. The maximum deflection in $p4$-like plate is formed in the centre of the assembly and the contours of the displacements have a "circular" shape. The lowest maximum deflection of 0.160 mm is in $p4$-like plate, the highest in $p1$-like plate at 1.66 mm.

at the edges of the frame. In these areas, the stress distribution differs notably between assemblies and monolithic plates. Assemblies transfer loading over specific blocks and relatively continuously along the block edges, whereas plates are supported locally at each sharp corner of the frame.

The results show that the variation of stress distribution in the $p4$ is more optimal compared to pg and $p1$, making it the best of the three options for this particular case. The blocks transferring forces to the frame in $p4$ are the least stressed, mostly falling within the green region (up to 11.5 MPa). In contrast, some marginal blocks in pg are stressed to around 19 MPa, while in $p1$ these blocks reach over 30 MPa.

As expected, we observe that the load transfer mechanisms in the regime of compressive stresses are qualitatively similar to those of a monolithic plate, while the load transfer significantly differs in case of tensile stresses. The reason for this lies in the fact that the gap between neighbouring blocks opens, and thus, contact is lost.

In civil engineering, the assemblies presented in this paper could be used, for example, as ceilings. Typically, such ceilings are made

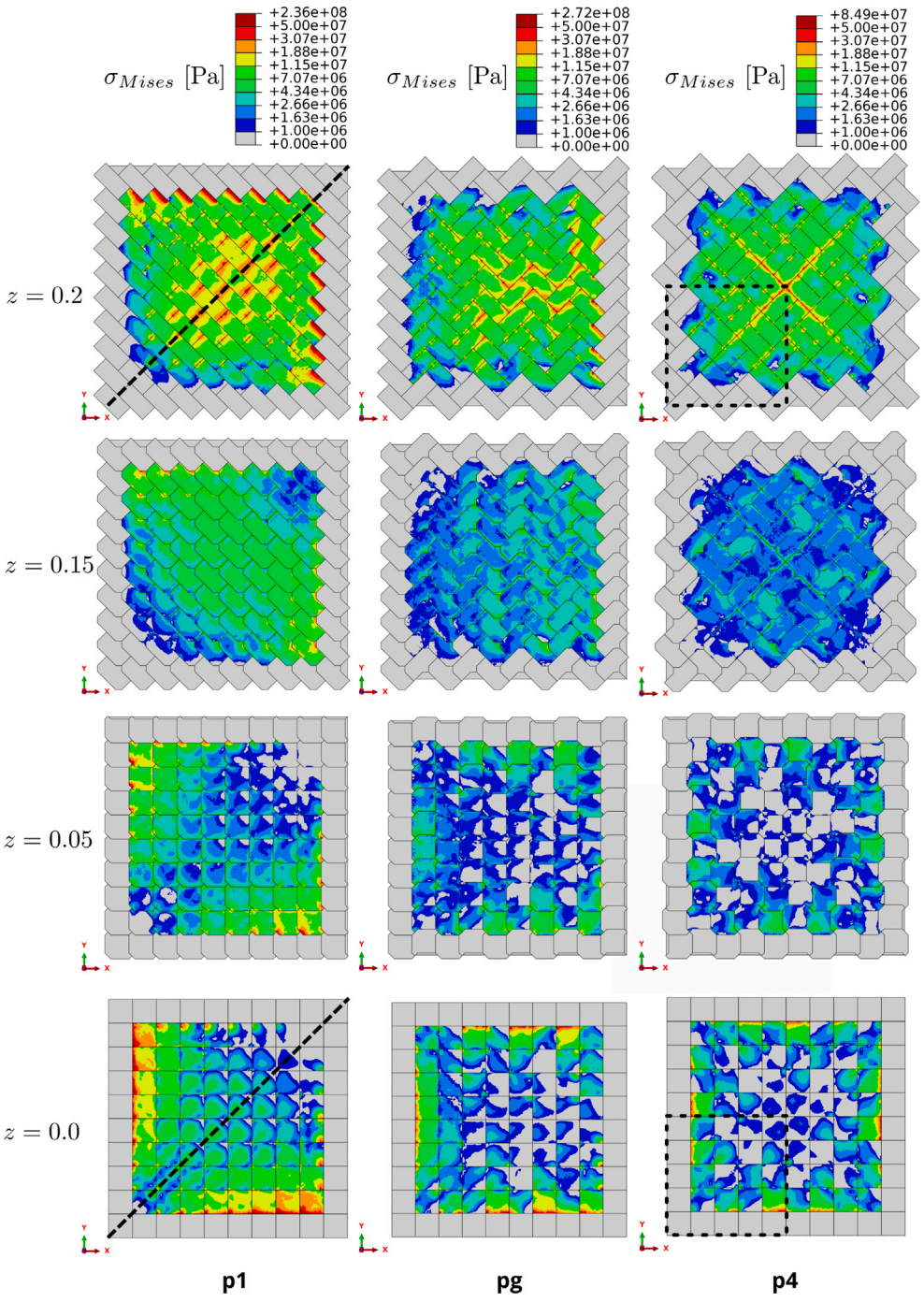

Fig. 16. Von Mises stress distributions in four planes of the TIA ($z = 0.0$ m, $z = 0.05$ m, $z = 0.15$ m and $z = 0.2$ m). The results show that different block arrangements strongly influence the stress distribution in the assembly. The highest von Mises stresses occur at the contacts between the blocks. Due to the symmetry of the Versatile Block and the assemblies, symmetry can also be observed in the stress distribution. For instance, in the $p4$ assembly, the four-fold rotational symmetry of the underlying wallpaper symmetry is still present in the stress distribution as highlighted by the black-square. Moreover, in the $p1$ assembly we see a reflection symmetry along the diagonal highlighted by the black-line. The case pg is more involved as the assembly is arranged using glide reflections this leads to a shift of the high stresses at the frame (note that a glide reflection is composed of a reflection together with a translation/shift). Below the middle plane $z = 0.1$ m the most blocks in the assemblies are less stressed compared to the same regions in the monolithic plates. This is because the gap between neighbouring blocks opens, causing a loss of contact. TIA transfer loading over specific blocks and relatively continuously along the block edges.

of concrete, a material that can withstand high compressive but low tensile loads. A solid plate loaded in the transverse direction will bend, resulting in compression in the upper and tension in the lower half of the plate, which is not desirable. To investigate the behaviour of TIA with respect to this problem, we plotted the normal stress field in y direction (see Fig. 18(a)), which is in our case the first indicator of tension or compression in the material. We can see that the negative stress predominates in the top planes (above $z = 0.1$ m) in all three TIA. The regions of the highest compressive stresses range from -7 to well over -100 MPa. In the bottom plane ($z = 0.0$ m), where the highest tensile stresses are to be expected, these remain in the range between 0 and 2 MPa. Comparing this result with the corresponding

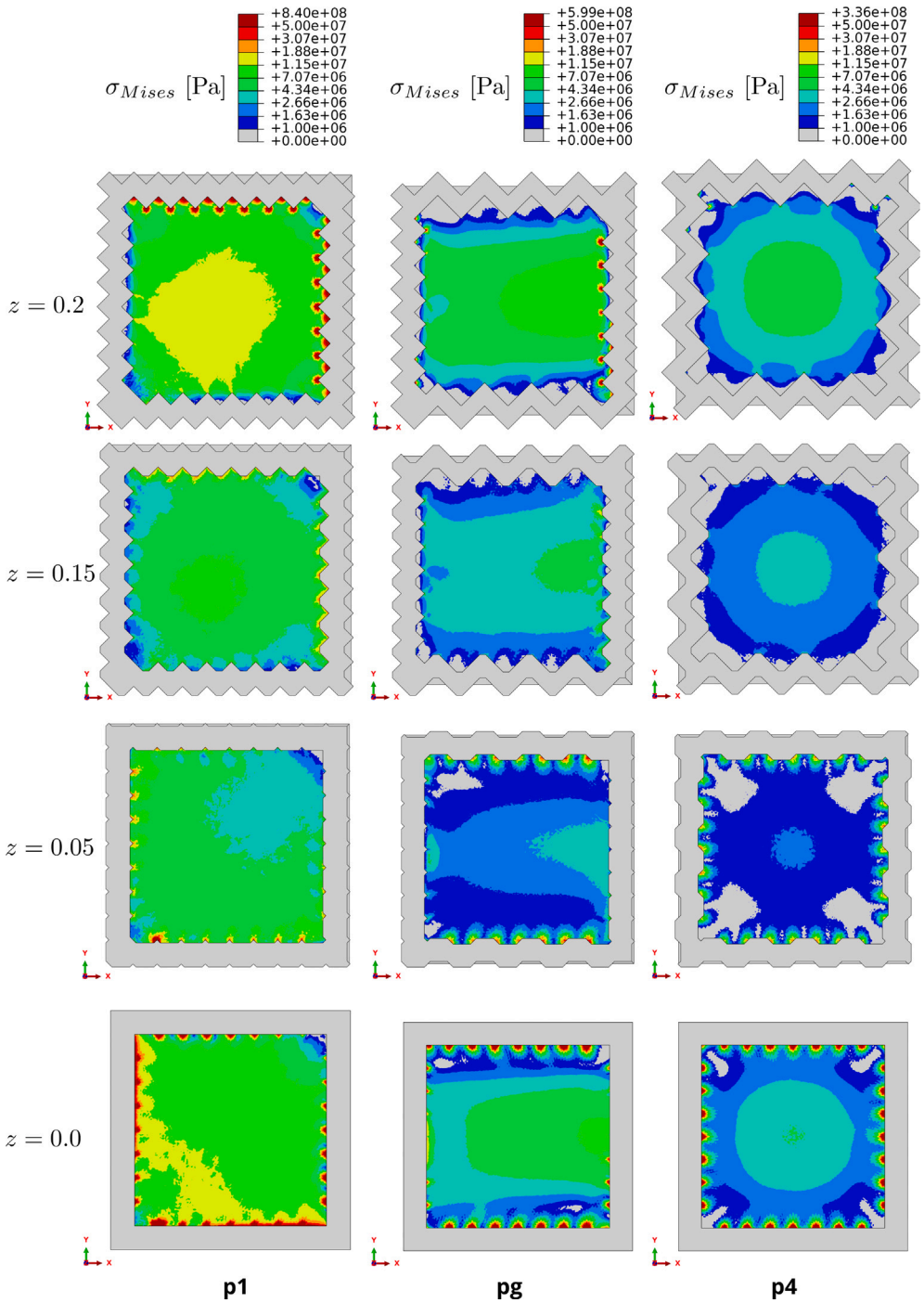

Fig. 17. Von Mises stress distributions in the four planes of the monolithic plates ($z = 0.0$ m, $z = 0.05$ m, $z = 0.15$ m and $z = 0.2$ m). Monolithic plates are supported locally at each sharp corner of the frame, where the highest von Mises stresses also occur. In comparison to the TIA the stress distributions in monolithic plates are continuous.

solid plates (Fig. 18(b)), where the highest compressive stresses range from −4 to −10 MPa and the highest tensile stresses are between 1 and 10 MPa, we can conclude that such TIA reduce undesired tensile stresses in the blocks. This can be advantageous, as less or even no reinforcement of the assembly may be required in practical realisation. However, it should be noted that due to the complex geometry of the Versatile Blocks, a complete reduction of the positive stresses in the blocks cannot be achieved.

5. Discussion

In this paper, we confirmed the hypothesis that the arrangement of blocks in a TIA has a significant influence on the overall structural behaviour such as its point of deflection, the load transfer mechanisms, as well as stress distribution. This is verified by comparing three different symmetric arrangements of the Versatile Block by FEM analyses. Moreover, by comparison with a monolithic plate, we demonstrated that the structural behaviour of TIA is qualitatively and quantitatively in the same order of magnitude. Further, we developed a combinatorial tool, called Interlocking Flows, that is capable of pre-evaluating the load transfer onto the frame. Intuitively, one would think that all

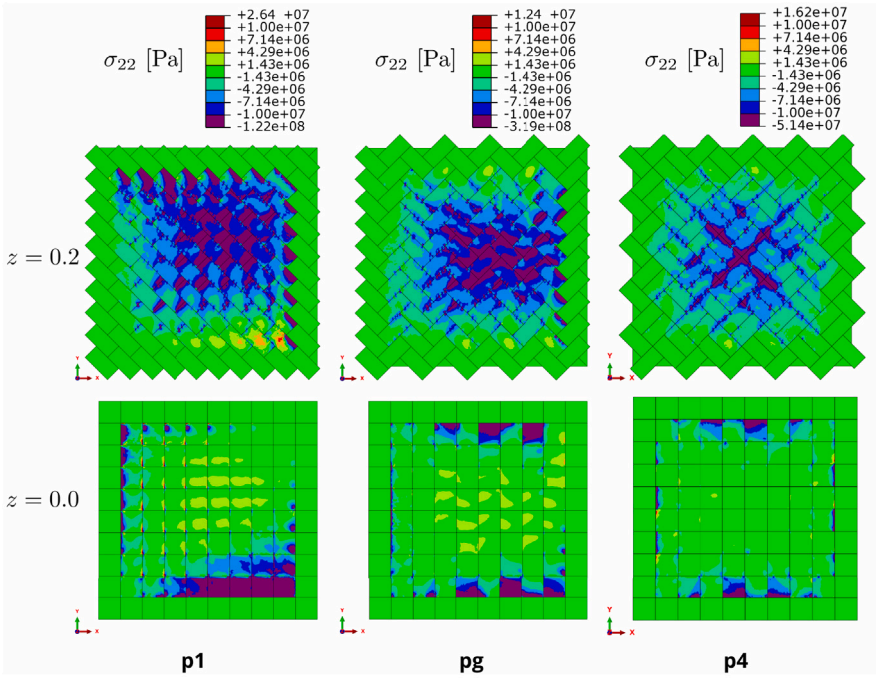

(a) TIA

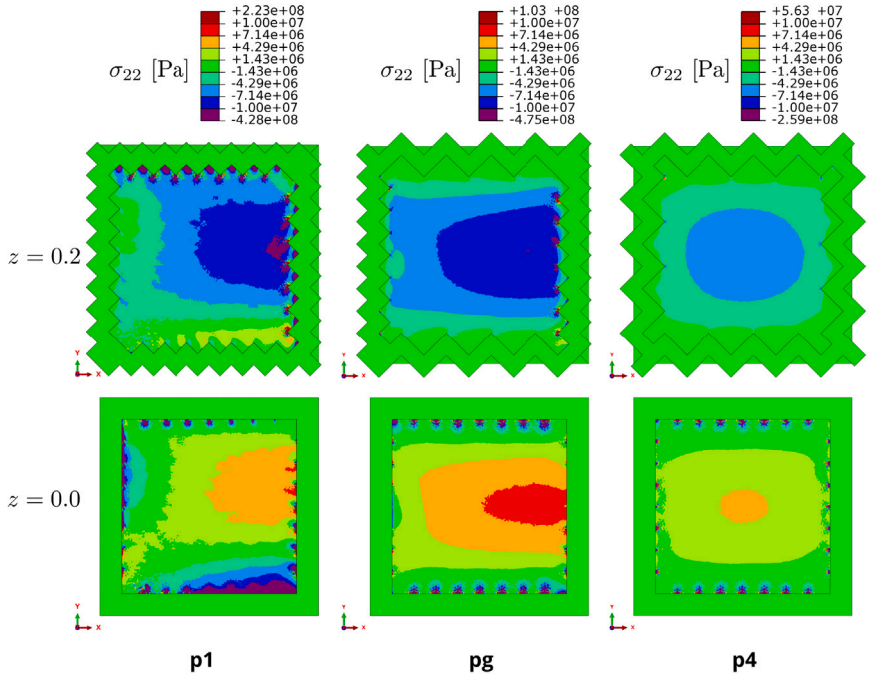

(b) Monolithic plates

Fig. 18. Normal stress field in the y-direction of the TIA and monolithic plates. Negative stress predominates in the top planes (above $z = 0.1$ m) across all three TIAs, with the highest compressive stresses ranging from −7 to well over −100 MPa. In contrast, the bottom plane ($z = 0.0$ m) exhibits stresses between 0 and 2 MPa. Compared to solid plates, where compressive stresses range from −4 to −10 MPa and tensile stresses from 1 to 10 MPa, TIA effectively reduce undesirable tensile stresses in the blocks.

peripheral blocks would be equally involved in transferring the external load to the frame. Both the combinatorial and numerical results show that this is not the case. The load is applied to the frame in a patterned manner, whereas the monolithic plate distributes the load continuously along the frame. In summary, we showed that by exploiting the rich combinatorial theory of the Versatile Block we obtain several interlocking assemblies with key differences. This can be exploited to custom-tailor interlocking assemblies for particular applications.

Another factor influencing the performance of the topological interlocking assembly is the distance between the top and bottom plane of the planar assembly. In order to design material minimised components, the mechanical performance of relatively thin assemblies should be investigated. As mentioned in Section 4 the scaling matrix for the Versatile Block was chosen according to Akpanya et al. (2023b) to guarantee versatility. Since the focus in this work lies on planar assemblies, the blocks could also be considered without top and bottom surface for lightweight structures. The influence of these scaling parameters as well as hollowing blocks on the overall mechanical response of the assembly was not examined. This was beyond the scope of this work.

The sharp edges of the geometry of the Versatile Block are responsible for stress spikes, see Fig. 14. This leads to the question of how to modify the geometry of the block from an engineering perspective in order to reduce these stress singularities. This question should be considered for further investigations.

In the simulation, friction was ignored to emphasise the interlocking effect. The results of the simulations (where friction is neglected) show that the proposed geometry under deformation is fully capable of self-interlocking and is therefore a promising candidate for practical use. Of course, in reality such (frictionless) conditions are not possible. Friction has a big impact on the overall behaviour of assembled systems and should therefore be taken into account in future work. Nevertheless, these results guarantee that the blocks cannot slip out of the assembly, as long as the deformation is not too large. The results also suggest that assemblies made from this geometry might perform quite stably even if one or more blocks are missing. This should, of course, also be investigated in future work.

In the context of this paper, a load has been applied evenly to the top plane in all assemblies in order to obtain a comparison of the different arrangement strategies. Considering different load cases should also be considered in future work.

In Fig. 12, we observe that the results of the Interlocking Flow model, which predicts force transfer from the assembly to the frame, are in good agreement with the contact pressure between the blocks and the frame obtained from the FEM analysis. This comparison indicates the reliability of Interlocking Flow method. Since FEM simulations are in general not as cost- and time-efficient, the Interlocking Flow method has significant potential for obtaining an initial evaluation of load transfer within the assembly. For future research, this discrete evaluation criterion needs to be investigated further, verified and developed.

CRediT authorship contribution statement

Tom Goertzen: Conceptualization, Formal analysis, Investigation, Software, Validation, Visualization, Writing – original draft, Writing – review & editing. **Domen Macek:** Conceptualization, Formal analysis, Investigation, Software, Validation, Visualization, Writing – original draft, Writing – review & editing. **Lukas Schnelle:** Software, Visualization, Writing – original draft, Writing – review & editing. **Meike Weiß:** Writing – original draft, Writing – review & editing. **Stefanie Reese:** Funding acquisition, Supervision. **Hagen Holthusen:** Funding acquisition, Supervision, Writing – review & editing. **Alice C. Niemeyer:** Conceptualization, Funding acquisition, Supervision, Writing – original draft, Writing – review & editing.

Declaration of competing interest

The authors declare that they have no known competing financial interests or personal relationships that could have appeared to influence the work reported in this paper.

Acknowledgements

The authors gratefully acknowledge funding by the Deutsche Forschungsgemeinschaft (DFG, German Research Foundation) in the framework of the Collaborative Research Centre CRC/TRR 280 “Design Strategies for Material-Minimized Carbon Reinforced Concrete Structures – Principles of a New Approach to Construction” (project ID 417002380). The authors thank Max Horn and Katharina Martin for their very valuable comments and advice. We also thank the anonymous reviewers for their suggestions, many of which were very helpful.

Appendix A. Software usage

The interlocking assemblies are generated using the SimplicialSurfaces Package Niemeyer et al. (2021) for GAP (2022). Here, we generate the different assemblies by first defining and rotating a single Versatile Block to all four possible orientations that can occur in a planar assembly. Then we create the assemblies given by the wallpaper groups of the three topological interlocking assemblies as described in Section 2. We divide the assembly into the outermost perimeter of blocks that we use as the frame. These assemblies are then exported as individual .stl files, which after a second conversion to .step files can be imported as geometries into Abaqus. This is done individually to allow easier application of the boundary conditions, but has no effect on the geometry as a whole. We use a 10×10 grid of 100 blocks in each of the periodic interlocking assemblies.

Appendix B. Wallpaper groups

Wallpaper groups can be seen as a mathematical formulation of symmetries of certain doubly periodic repeating patterns in a 2-dimensional plane. They are also known as 2-dimensional crystallographic groups and contain rotations, reflections and translations respecting the repeated pattern. For the repetition of the pattern, we need a translation which describes the offset of the pattern, denoted as a vector in $\mathbb{R}^2$. Furthermore, a rotation or reflection can be described by a matrix

$$\begin{pmatrix} \cos(\theta) & -\sin(\theta) \\ \sin(\theta) & \cos(\theta) \end{pmatrix} \text{ or } \begin{pmatrix} \cos(\theta) & \sin(\theta) \\ \sin(\theta) & -\cos(\theta) \end{pmatrix}$$

respectively, where θ is the angle of rotation. A reflection means, we mirror at a plane through the origin with a certain angle. It turns out, that θ can only have the values $0°, 60°, 90°, 120°$, and $180°$ (see crystallographic restriction theorem Armstrong, 1988, Chapter 25). A single symmetry of a repeating pattern can therefore be described as a pair (M, v), where M is a rotation or reflection matrix and v is an (offset) vector as before. We call such an object an *isometry*. An isometry (M, v) acts on $\mathbb{R}^2$ as a function

$$f_{(M,v)} : \mathbb{R}^2 \to \mathbb{R}^2, x = \begin{pmatrix} x_1 \\ x_2 \end{pmatrix} \mapsto M \cdot \begin{pmatrix} x_1 \\ x_2 \end{pmatrix} + v,$$

whereas the product of two isometries $(M_1, v_1), (M_2, v_2)$ is defined as follows:

$$(M_2, v_2) \circ (M_1, v_1) := (M_2 \cdot M_1, M_2 \cdot v_1 + v_2)$$

where $\cdot$ denotes the matrix–vector multiplication. Every wallpaper group is generated by a finite set of isometries, see Szczepański (2012), i.e. all elements of the group are products of these isometries. To be more precise, we define a wallpaper group (also called wallpaper symmetry) along the same lines as Armstrong (1988) as follows:

Definition B.1. Let E(2) denote the group of isometries of the Euclidean plane $\mathbb{R}^2$. A subgroup

$$\Gamma := \langle (M_1, v_1), \dots, (M_r, v_r) \rangle \subseteq \mathrm{E}(2)$$

such that M_i is a rotation or reflection matrix and $v_i \in \mathbb{R}^2$ for $1 \leq i \leq r$ is called *wallpaper group* if

(i) the set $\{v_1, \dots, v_r\}$ contains two linearly independents vectors and
(ii) there are only finitely many matrices that can be written as $M = M_{i_1} \cdot \dots \cdot M_{i_k}$ with $M_{i_j} \in \{M_1, \dots, M_r\}$, $1 \leq j \leq k$ (i.e. the M_i span a finite *point group*).

In this definition, (i) ensures that we can find a set $D \subseteq \mathbb{R}^2$ (called fundamental domain) such that for any point x in the plane, there is a point $y \in D$ and an isometry in Γ that maps x to y. (ii) ensures that we obtain a repeating pattern F, also known as *fundamental domain*. It

turns out, that there are only 17 wallpaper groups (up to isomorphism), see Armstrong (1988).

In this paper, we only consider the three wallpaper groups $p1$, pg and $p4$. Here, we follow the international crystallographic notation Aroyo (2016) for the names of the wallpaper groups. The group $p1$ can be characterised by only allowing translations as both matrices are the identity:

$$p1 := \left\langle \left(\begin{pmatrix} 1 & 0 \\ 0 & 1 \end{pmatrix}, \begin{pmatrix} 1 \\ -1 \end{pmatrix} \right), \left(\begin{pmatrix} 1 & 0 \\ 0 & 1 \end{pmatrix}, \begin{pmatrix} 1 \\ 1 \end{pmatrix} \right) \right\rangle.$$

In the group pg we have an additional (glide-)reflection in the first generator. After applying this matrix twice it becomes the identity and therefore the fundamental domain F is oriented in two different ways in a tiling with pg-symmetry :

$$pg := \left\langle \left(\begin{pmatrix} 0 & -1 \\ -1 & 0 \end{pmatrix}, \begin{pmatrix} 2 \\ 0 \end{pmatrix} \right), \left(\begin{pmatrix} 1 & 0 \\ 0 & 1 \end{pmatrix}, \begin{pmatrix} 1 \\ 1 \end{pmatrix} \right) \right\rangle.$$

Compared to the one reflection in pg we have a rotation associated to both generators in the group $p4$. However, due to the rotation matrices becoming the identity after being applied four times, the fundamental domain F can be oriented in exactly four ways in a tiling with $p4$-symmetry:

$$p4 := \left\langle \left(\begin{pmatrix} 0 & 1 \\ -1 & 0 \end{pmatrix}, \begin{pmatrix} 0 \\ 2 \end{pmatrix} \right), \left(\begin{pmatrix} 0 & -1 \\ 1 & 0 \end{pmatrix}, \begin{pmatrix} 0 \\ -2 \end{pmatrix} \right), \left(\begin{pmatrix} -1 & 0 \\ 0 & -1 \end{pmatrix}, \begin{pmatrix} 0 \\ 0 \end{pmatrix} \right) \right\rangle.$$

References

Akleman, Ergun, Krishnamurthy, Vinayak R., Fu, Chia-An, Subramanian, Sai Ganesh, Ebert, Matthew, Eng, Matthew, Starrett, Courtney, Panchal, Haard, 2020. Generalized abeille tiles: Topologically interlocked space-filling shapes generated based on fabric symmetries. Comput. Graph. 89, 156–166. http://dx.doi.org/10.1016/j.cag.2020.05.016.

Akpanya, Reymond, Goertzen, Tom, Niemeyer, Alice C., 2023a. A group-theoretic approach for constructing spherical-interlocking assemblies. In: Xie, Y.M., Burry, J., Lee, T.U., Ma, J. (Eds.), Proceedings of the IASS Annual Symposium 2023: Integration of Design and Fabrication. Vol. 7, International Association for Shell and Spatial Structures (IASS), Melbourne, Australia, pp. 470–480.

Akpanya, Reymond, Goertzen, Tom, Wiesenhuetter, Sebastian, Niemeyer, Alice C., Noennig, Jörg, 2023b. Topological interlocking, truchet tiles and self-assemblies: A construction-kit for civil engineering design. In: Holdener, Judy, Torrence, Eve, Fong, Chamberlain, Seaton, Katherine (Eds.), Proceedings of Bridges 2023: Mathematics, Art, Music, Architecture, Culture. Tessellations Publishing, Phoenix, Arizona, ISBN: 978-1-938664-45-8, pp. 61–68.

Armstrong, M.A., 1988. Groups and Symmetry. In: Undergraduate Texts in Mathematics, Springer-Verlag, New York, ISBN: 0-387-96675-7, http://dx.doi.org/10.1007/978-1-4757-4034-9.

Aroyo, Mois I. (Ed.), 2016. International Tables for Crystallography, Volume a: Space-Group Symmetry, sixth ed. Vol. A, Wiley, ISBN: 978-0-470-97423-0, http://dx.doi.org/10.1107/97809553602060000114.

Djumas, Lee, Simon, George P., Estrin, Yuri, Molotnikov, Andrey, 2017. Deformation mechanics of non-planar topologically interlocked assemblies with structural hierarchy and varying geometry. Scientific Reports 7 (1), 11844. http://dx.doi.org/10.1038/s41598-017-12147-3.

Dyskin, A.V., Estrin, Y., Kanel-Belov, A.J., Pasternak, E., 2001a. A new concept in design of materials and structures: assemblies of interlocked tetrahedron-shaped elements. Scr. Mater. 44 (12), 2689–2694. http://dx.doi.org/10.1016/S1359-6462(01)00968-X.

Dyskin, A.V., Estrin, Y., Kanel-Belov, A.J., Pasternak, E., 2001b. Toughening by fragmentation—How topology helps. Adv. Eng. Mater. 3 (11), 885–888. http://dx.doi.org/10.1002/1527-2648(200111)3:11<885::AID-ADEM885>3.0.CO;2-P.

Dyskin, A.V., Estrin, Y., Kanel-Belov, A.J., Pasternak, E., 2003a. Topological interlocking of platonic solids: A way to new materials and structures. Phil. Mag. Lett. 83 (3), 197–203. http://dx.doi.org/10.1080/0950083031000065226.

Dyskin, A.V., Estrin, Yuri, Pasternak, E., 2019. Topological interlocking materials. In: Estrin, Yuri, Bréchet, Yves, Dunlop, John, Fratzl, Peter (Eds.), Architectured Materials in Nature and Engineering: Archimats. Springer International Publishing, Cham, ISBN: 978-3-030-11942-3, pp. 23–49. http://dx.doi.org/10.1007/978-3-030-11942-3_2.

Dyskin, A.V., Estrin, Y., Pasternak, E., Khor, H.C., Kanel-Belov, A.J., 2003b. Fracture resistant structures based on topological interlocking with non-planar contacts. Adv. Eng. Mater. 5 (3), 116–119. http://dx.doi.org/10.1002/adem.200390016.

Ebert, Matthew, Akleman, Ergun, Krishnamurthy, Vinayak, Kulagin, Roman, Estrin, Yuri, 2023. VoroNoodles: Topological interlocking with helical layered 2-honeycombs. Adv. Eng. Mater. 2300831. http://dx.doi.org/10.1002/adem.202300831.

Estrin, Yuri, Krishnamurthy, Vinayak R., Akleman, Ergun, 2021. Design of architectured materials based on topological and geometrical interlocking. J. Mater. Res. Technol. 15, 1165–1178. http://dx.doi.org/10.1016/j.jmrt.2021.08.064.

Feldfogel, Shai, Karapiperis, Konstantinos, Andrade, Jose, Kammer, David S., 2023. Scaling, saturation, and upper bounds in the failure of topologically interlocked structures. Int. J. Solids Struct. 269, 112228. http://dx.doi.org/10.1016/j.ijsolstr.2023.112228.

Feldfogel, Shai, Karapiperis, Konstantinos, Andrade, Jose, Kammer, David S., 2024a. A discretization-convergent level-set-discrete-element-method using a continuum-based contact formulation. Internat. J. Numer. Methods Engrg. 125 (5), e7400. http://dx.doi.org/10.1002/nme.7400.

Feldfogel, Shai, Karapiperis, Konstantinos, Andrade, Jose, Kammer, David S., 2024b. Failure of topologically interlocked structures — a level-set-DEM approach. Eur. J. Mech. A Solids 103, 105156. http://dx.doi.org/10.1016/j.euromechsol.2023.105156.

Feng, Yuezhong, Siegmund, Thomas, Habtour, Ed, Riddick, Jaret, 2015. Impact mechanics of topologically interlocked material assemblies. Int. J. Impact Eng. 75, 140–149. http://dx.doi.org/10.1016/j.ijimpeng.2014.08.003.

Frézier, Amédée François, 1738. La Theorie et la Pratique de la Coupe des Pierres et Des Bois, Pour la Construction des Voutes et Autres Parties Des Bâtimens Civils & Militaires, Ou Traité de Stereotomie a l'Usage de l'Architecture, vol. 2, Doulsseker.

Gallon, J.-G., 1735. Machines et inventions approuvées par l'académie royale des sciences depuis son établissement jusqu'à present; avec leur description. Acad. R. Sci..

GAP, GAP – groups, algorithms, and programming, Version 4.12.2. https://www.gap-system.org, Dec 18.

Glickman, Michael, 1984. The G-block system of vertically interlocking paving. In: Second International Conference on Concrete Block Paving. pp. 10–12.

Goertzen, Tom, 2024a. Constructing interlocking assemblies with crystallographic symmetries. http://dx.doi.org/10.48550/arXiv.2405.15080, arXiv e-prints, art. arXiv:2405.15080.

Goertzen, Tom, 2024b. Mathematical foundations of interlocking assemblies. http://dx.doi.org/10.48550/arXiv.2405.17644, arXiv e-prints, art. arXiv:2405.17644.

Goertzen, Tom, Macek, Domen, Schnelle, Lukas, Weiß, Meike, Reese, Stefanie, Holthusen, Hagen, Niemeyer, Alice C., 2023. Mechanical comparison of arrangement strategies for topological interlocking assemblies: Abaqus input files.

Goertzen, Tom, Niemeyer, Alice C., Plesken, Wilhelm, 2022. Topological interlocking via symmetry. In: Stokkeland, S., Braarud, H.C (Eds.), 6th Fib International Congress on Concrete Innovation for Sustainability, 2022; Oslo; Norway. pp. 1235–1244.

Harsono, Kevin, Shih, Shen-Guan, Wagiri, Felicia, Alfred, William, 2023. Integration of design and performance evaluation for reusable osteomorphic-block masonry. Nexus Netw. J. http://dx.doi.org/10.1007/s00004-023-00756-7.

Kanel-Belov, A.J., Dyskin, A.V., Estrin, Y., Pasternak, E., Ivanov-Pogodaev, I.A., 2010. Interlocking of convex polyhedra: towards a geometric theory of fragmented solids. Mosc. Math. J. 10 (2), 337–342. http://dx.doi.org/10.17323/1609-4514-2010-10-2-337-342, 478–479.

Khandelwal, S., Siegmund, T., Cipra, R.J., Bolton, J.S., 2012. Transverse loading of cellular topologically interlocked materials. International Journal of Solids and Structures 49 (18), 2394–2403. http://dx.doi.org/10.1016/j.ijsolstr.2012.04.035.

Khandelwal, S., Siegmund, T., Cipra, R.J., Bolton, J.S., 2013. Scaling of the Elastic Behavior of Two-Dimensional Topologically Interlocked Materials Under Transverse Loading. Journal of Applied Mechanics 81 (031011), http://dx.doi.org/10.1115/1.4024907.

Kim, Dong Young, Siegmund, Thomas, 2021. Mechanics and design of topologically interlocked irregular quadrilateral tessellations. Mater. Des. 212, 110155. http://dx.doi.org/10.1016/j.matdes.2021.110155.

Koureas, Ioannis, Pundir, Mohit, Feldfogel, Shai, Kammer, David S., 2022. On the failure of beam-like topologically interlocked structures. Int. J. Solids Struct. 259, 112029. http://dx.doi.org/10.1016/j.ijsolstr.2022.112029.

Koureas, Ioannis, Pundir, Mohit, Feldfogel, Shai, Kammer, David S., 2023. Beam-like topologically interlocked structures with hierarchical interlocking. J. Appl. Mech. 90 (081008), http://dx.doi.org/10.1115/1.4062348.

Krause, T., Molotnikov, A., Carlesso, M., Rente, J., Rezwan, K., Estrin, Y., Koch, D., 2012. Mechanical properties of topologically interlocked structures with elements produced by freeze gelation of ceramic slurries. Adv. Eng. Mater. 14 (5), 335–341. http://dx.doi.org/10.1002/adem.201100244.

Laursen, Tod A., 2002. Computational Contact and Impact Mechanics. Springer, Berlin, Heidelberg, http://dx.doi.org/10.1007/978-3-662-04864-1.

Mirkhalaf, Mohammad, Zhou, Tao, Barthelat, Francois, 2018. Simultaneous improvements of strength and toughness in topologically interlocked ceramics. Proc. Natl. Acad. Sci. 115 (37), 9128–9133. http://dx.doi.org/10.1073/pnas.1807272115.

Mullins, Cassie, Ebert, Matthew, Akleman, Ergun, Krishnamurthy, Vinayak, 2022. Voronoi spaghetti & VoroNoodles: Topologically interlocked, space-filling, corrugated & congruent tiles. In: SIGGRAPH Asia 2022 Technical Communications. SA '22, Association for Computing Machinery, New York, NY, USA, ISBN: 978-1-4503-9465-9, http://dx.doi.org/10.1145/3550340.3564229.

Niemeyer, A.C., Baumeister, M., Akpanya, R., Görtzen, T., Weiß, M., 2021. SimplicialSurfaces, computing with simplicial surfaces and folding processes. Version 0.6. https://github.com/gap-packages/SimplicialSurfaces. GAP package.

Rezaee Javan, Anooshe, Seifi, Hamed, Lin, Xiaoshan, Xie, Yi Min, 2020. Mechanical behaviour of composite structures made of topologically interlocking concrete bricks with soft interfaces. Mater. Des. 186, 108347. http://dx.doi.org/10.1016/j.matdes.2019.108347.

Rezaee Javan, A., Seifi, H., Xu, S., Lin, X., Xie, Y.M., 2018. Impact behaviour of plate-like assemblies made of new and existing interlocking bricks: A comparative study. Int. J. Impact Eng. 116, 79–93. http://dx.doi.org/10.1016/j.ijimpeng.2018.02.008.

Rezaee Javan, A., Seifi, H., Xu, S., Ruan, D., Xie, Y.M., 2017. The impact behaviour of plate-like assemblies made of new interlocking bricks: An experimental study. Mater. Des. 134, 361–373. http://dx.doi.org/10.1016/j.matdes.2017.08.056.

Rezaee Javan, Anooshe, Seifi, Hamed, Xu, Shanqing, Xie, Yi Min, 2016. Design of a new type of interlocking brick and evaluation of its dynamic performance. In: Proceedings of IASS Annual Symposia, IASS 2016 Tokyo Symposium: Spatial Structures in the 21st Century – New Approaches, Materials & Construction Methods. International Association for Shell and Spatial Structures (IASS), International Association for Shell and Spatial Structures (IASS), Tokyo, Japan, pp. 1–8.

Schaare, S., Dyskin, A.V., Estrin, Y., Arndt, S., Pasternak, E., Kanel-Belov, A., 2008. Point loading of assemblies of interlocked cube-shaped elements. Internat. J. Engrg. Sci. 46 (12), 1228–1238. http://dx.doi.org/10.1016/j.ijengsci.2008.06.012.

Schaare, Stephan, Riehemann, Werner, Estrin, Yuri, 2009. Damping properties of an assembly of topologically interlocked cubes. Mater. Sci. Eng. A 521–522, 380–383. http://dx.doi.org/10.1016/j.msea.2008.10.069.

Short, M., Siegmund, T., 2019. Scaling, growth, and size effects on the mechanical behavior of a topologically interlocking material based on tetrahedra elements. J. Appl. Mech. 86 (111007), http://dx.doi.org/10.1115/1.4044025.

Siegmund, Thomas, Barthelat, Francois, Cipra, Raymond, Habtour, Ed, Riddick, Jaret, 2016. Manufacture and mechanics of topologically interlocked material assemblies. Appl. Mech. Rev. 68 (040803), http://dx.doi.org/10.1115/1.4033967.

Smith, Cyril Stanley, Boucher, Pauline, 1987. The tiling patterns of sebastien truchet and the topology of structural hierarchy. Leonardo 20 (4), 373–385.

Subramanian, Sai Ganesh, Eng, Mathew, Krishnamurthy, Vinayak R., Akleman, Ergun, 2019. Delaunay Lofts: A biologically inspired approach for modeling space filling modular structures. Comput. Graph. 82, 73–83. http://dx.doi.org/10.1016/j.cag.2019.05.021.

Szczepański, Andrzej, 2012. Geometry of Crystallographic Groups. In: Algebra and Discrete Mathematics, vol. 4, World Scientific Publishing Co. Pte. Ltd, Hackensack, NJ, ISBN: 978-981-4412-25-4, http://dx.doi.org/10.1142/8519.

Ullmann, Silvan, Kammer, David S., Feldfogel, Shai, 2023. The deflection limit of slab-like topologically interlocked structures. J. Appl. Mech. 91 (021004), http://dx.doi.org/10.1115/1.4063345.

Wang, Ziqi, Song, Peng, Pauly, Mark, 2018. DESIA: A general framework for designing interlocking assemblies. ACM Trans. Graph. 37 (6), http://dx.doi.org/10.1145/3272127.3275034.

Weizmann, Michael, Amir, Oded, Grobman, Yasha Jacob, 2021. The effect of block geometry on structural behavior of topological interlocking assemblies. Autom. Constr. 128, 103717. http://dx.doi.org/10.1016/j.autcon.2021.103717.

Williams, Andrew, Siegmund, Thomas, 2021. Mechanics of topologically interlocked material systems under point load: Archimedean and Laves tiling. Int. J. Mech. Sci. 190, 106016. http://dx.doi.org/10.1016/j.ijmecsci.2020.106016.

Wilson, Randall H., 1992. On Geometric Assembly Planning (Ph.D. thesis). Stanford, CA, USA.

Wilson, Randall H., Latombe, Jean-Claude, 1994. Geometric reasoning about mechanical assembly. Artificial Intelligence 71 (2), 371–396. http://dx.doi.org/10.1016/0004-3702(94)90048-5.

Wriggers, Peter, 2006. Computational Contact Mechanics. Springer, Berlin, Heidelberg, http://dx.doi.org/10.1007/978-3-540-32609-0.

Wriggers, Peter, 2008. Nonlinear Finite Element Methods. Springer, Berlin, Heidelberg, http://dx.doi.org/10.1007/978-3-540-71001-1.

Yong, Hsien Ta David, 2011. Utilisation of Topologically-Interlocking Osteomorphic Blocks for Multi-Purpose Civil Construction (Doctoral Thesis).

Zienkiewicz, Olek C., Taylor, Robert L., Zhu, Jian Z., 2005. The Finite Element Method: Its Basis and Fundamentals. Elsevier.